JOURNAL OF GEOPHYSICAL RESEARCH, VOL. 105, NO. D1, PAGES 1563–1583, JANUARY 20, 2000

Measurements of trace gases and photolysis frequencies during SLOPE96 and a coarse estimate of the local OH concentration from HNO_3 formation

Hans-Werner Pätz,[1] Uli Corsmeier,[2] Konrad Glaser,[3] Ulrich Vogt,[3] Norbert Kalthoff,[2] Dieter Klemp,[1] Bita Kolahgar,[1] Ansgar Lerner,[1] Bruno Neininger,[4] Thomas Schmitz,[1] Martin G. Schultz,[1,5] Jana Slemr,[6] and Andreas Volz-Thomas[1]

Abstract. The Schauinsland Ozone Precursor Experiment (SLOPE96) campaign was conducted in June 1996 to study the physicochemical transformation of pollutants and the production of photooxidants during transport from the city of Freiburg to the Schauinsland mountain. For this purpose, chemical surface measurements were made at the entrance of the valley Großes Tal, and close to the Schauinsland summit, at 1200 m altitude on a saddle at the end of the valley. In addition, measurements of ozone, NO_2, and meteorological parameters were made on two tethered balloons and aboard a small aircraft. This paper describes the experimental setup and the measurements of ozone, odd-nitrogen compounds, carbonyl compounds, CO, and photolysis frequencies made during SLOPE96. The various instruments used on the different platforms were harmonized on the basis of intercomparison experiments in order to achieve a consistent picture. Large precursor concentrations from the nearby city of Freiburg are transported to Schauinsland in a valley wind system during stagnant high-pressure conditions. These conditions occurred only on 2 days of the campaign, and only 1 day (June 5) was predictable enough to allow for deployment of the aircraft and the balloons. An OH concentration of $8–10 \times 10^6$ cm^{-3} is derived from the rate of change of HNO_3 and NO_2 on June 5 at Schauinsland (1.5–3 ppb NO_2; $J_{O1D} \approx 2 \times 10^{-5}$ s^{-1}), assuming quasi steady state and a homogeneous air mass. The ozone production rate as determined from the photostationary state of NO_x at Schauinsland reached maximum daily values between 15 and 60 ppb h^{-1} around noontime. On average, $P(O_3)$ comprised about 30% of the photolysis rate of NO_2. Similar to earlier observations at Schauinsland, a good correlation between $P(O_3)$ and the product of UV radiation and precursor concentrations was found.

1. Introduction

The Schauinsland Ozone Precursor Experiment (SLOPE96) campaign was conducted in June 1996 to study the transformation of trace gases in the plume of the city of Freiburg during transport to the Schauinsland mountain. The idea for SLOPE96 came from the long-term measurements of photooxidants and precursors that were made at Schauinsland within the framework of the former European Experiment on Transport and Transformation of Environmentally Relevant Trace Constituents in the Troposphere Over Europe (EUROTRAC) subproject Tropospheric Ozone Research (TOR) [*Kley et al.*, 1997]. From the long-term observations of ozone, peroxides, odd-nitrogen compounds, etc. it was found that the Schauinsland frequently received polluted air from the Upper Rhine Valley and the nearby city of Freiburg via a thermally driven valley wind system. SF_6 transport experiments subsequently showed that the dominant portion of the pollution is advected through the valley named Großes Tal.

The necessary meteorological situation for the valley wind system to be established is a high-pressure system over central Europe with weak easterly geostrophic flow over southern Germany. Because of the orographic structure of the steep and narrow valley Großes Tal, its rather thin population, and the absence of transit traffic, it is well suited for studying the dynamics of dispersion and chemical transformation during transport of an urban air mass into rural environments.

A first experiment was carried out in September 1992, with chemical measurements made at the entrance of the valley, in addition to those at Schauinsland. The results were used to derive the time-integrated OH concentration by simultaneously solving the continuity equation for a family of reactive hydrocarbons that had been measured at both sites [*Kramp and Volz-Thomas*, 1997]. The estimated OH concentration ($5–8 \times 10^6$ cm^{-3}) was relatively high in view of the accompanying NO_x mixing ratio (16–70 ppb), and the radical budget could not be closed on the basis of the known sources and sinks. Tracer experiments with SF_6 were made in the subsequent years in order to study the transport and dispersion. On the basis of

[1]Institut fur Chemie und Dynamik der Geosphare II, Forschungszentrum Jülich, Jülich, Germany.
[2]Institut fur Meteorologie und Klimaforschung, Forschungszentrum Karlsruhe, Karlsruhe, Germany.
[3]Institut für Verfahrenstechnik und Dampfkesselwesen, Universität Stuttgart, Stuttgart, Germany.
[4]MetAir AG, Illnau, Switzerland.
[5]Now at Max-Planck-Institut für Meteorologie, Hamburg, Germany.
[6]Fraunhofer Institut fur Atmospharische Umweltforschung, Garmisch-Partenkirchen, Germany.

Paper number 1999JD900918.
0148-0227/00/1999JD900918$09.00

Table 1. Field Sites in SLOPE96 and Institutions Responsible for the Measurements

Position in Figure 1	Abbreviation in Text	Institution	Acronym	Measuring System	Height, m asl
A	SL	Forschungszentrum Jülich-ICG2	ICG2	TOR station Schauinsland chemical measurements	1230
B		Uni Paderborn	UPb	meteorological tower	1060
C		Uni Paderborn	UPb	meteorological tower	980
D	KG	Forschungszentrum Geesthacht	GKSS	ozone LIDAR, SODAR	830
D	KG	Forschungszentrum Karlsruhe-Institut für Meteorologie und Klimaforschung	IMK	tethered balloon	830
E	MH	Fraunhoferinstitut für Atmosphärische Umweltforschung	IFU	IFU container	630
F	RE	Forschungszentrum Karlsruhe-Institut für Meteorologie und Klimaforschung	IMK	SODAR	980
G	RE	Uni Freiburg Geologisches Institut	MIF	meteorological tower	995
H	MS	Uni Freiburg Geologisches Institut	MIF	tethered balloon	495
I	K2	Uni Stuttgart-Institut für Statik und Dynamik der Luft- und Raumfahrt	IVD	launch site of airship	392
J	K2	Uni Stuttgart-Institut für Verfahrenstechnik und Dampfkesselwesen	IVD	tethered balloon	385
K	K1	Forschungszentrum Jülich-ICG2	ICG2	mobile laboratory chemical measurements	354
K	K1	Forschungszentrum Jülich-ASS	ASS	meteorological tower	354
K	K1	Max-Planck-Institut Hamburg	MPI HH	ozone LIDAR	354
K	K1	Uni Köln Meteorologisches Institut	MIK	SODAR	354
L	WW	Uni Freiburg Geologisches Institut	MIF	SODAR	330
M	WW	Forschungszentrum Karlsruhe-Institut für Meteorologie und Klimaforschung	IMK	radio sonde	327
X		Forschungszentrum Jülich-ASS	ASS	release sites for SF_6	
•		Forschungszentrum Jülich-ASS	ASS	sampling sites for SF_6	

these experiments the SLOPE96 campaign was planned. A large number of groups contributed chemical and meteorological measurements at several surface sites, on tethered balloons, a small airship, and a small aircraft (see Table 1). Calibration standards were regularly exchanged between different groups, and a comprehensive intercomparison was made after the campaign. The meteorological measurements are discussed in detail by *Kalthoff et al.* [this issue], and the measurements of volatile organic compounds (VOC) are described by B. Kolahgar et al. (unpublished manuscript, 1999). This paper describes the chemical measurements made during SLOPE96 at the two surface sites, on two tethered balloons, and aboard the aircraft, and provides a first analysis of NO_x and ozone chemistry.

2. Experiment

A map of the Schauinsland region which includes the different measurement sites is shown in Figure 1. Detailed chemical measurements were made at two surface sites: in Kappel (K1), a small village at the entrance to the valley, and at the TOR station Schauinsland (SL), near the top of the mountain. Vertical soundings with tethered balloons were made at four locations: O_3, NO_2, and meteorological parameters were measured by the Institut für Verfahrenstechnik und Dampfkesselwesen (IVD) at Kappel (K2), about 800 m south of the mobile laboratory; O_3 and meteorological parameters were measured by the Institut für Meteorologie und Klimaforschung (IMK) at Kohlengrund (KG), and meteorological parameters were measured at Rappeneck (RE) and at Molzhof (MS).

2.1. Surface Sites (SL and K1)

The analytical techniques used for the determination of trace gases and photolysis rates at the two surface sites Schauinsland and Kappel are summarized in Table 2. At the TOR station Schauinsland the analytical instruments were installed in an air-conditioned laboratory located on the upper floor of a three-storied building. The inlets were mounted 2 m above the roof of the building, 12 m aboveground. They were connected to the instruments via 5 m of 1/4 inch OD perfluoroalkoxy (PFA) tubing. At Kappel the equipment was installed in the air-conditioned mobile laboratory of Forschungszentrum Jülich (FZJ). The inlets and meteorological instruments were 10 m above the surface on a pneumatic mast.

2.1.1. O_3. Ozone was measured at both sites with UV absorption instruments (Thermo Environmental Instruments Inc., Model TE 49). PTFE filters (Millipore, type HA, 0.45 μm pore size) were installed in the inlets and exchanged every week. The comparability of the two ozone monitors was checked before the campaign using the transfer standard described below. The agreement was better than 2%.

2.1.2. CO. Carbon monoxide (CO) was measured at both sites by infrared filter correlation instruments (Thermo Environmental Instruments Inc., Model TE 48). In order to reduce the interference by atmospheric water vapor, Nafion driers were used in the inlet lines. The instrument's zero was determined every hour by passing the sample air through a hopcalite scrubber. Calibration was done with standard mixtures of 300 and 1010 ppb CO in air, respectively. The standards had been compared before the campaign with a certified National Institute of Standards and Technology (NIST) standard (1 ppm). The NIST standard was found to agree within 2% with standards of the National Center for Atmospheric Research [*Gerbig et al.*, 1996] and the National Oceanic and Atmospheric Administration (NOAA) Aeronomy Laboratory (J. S. Holloway et al., Airborne intercomparison of vacuum ultraviolet fluorescence and tunable diode laser absorption measurements

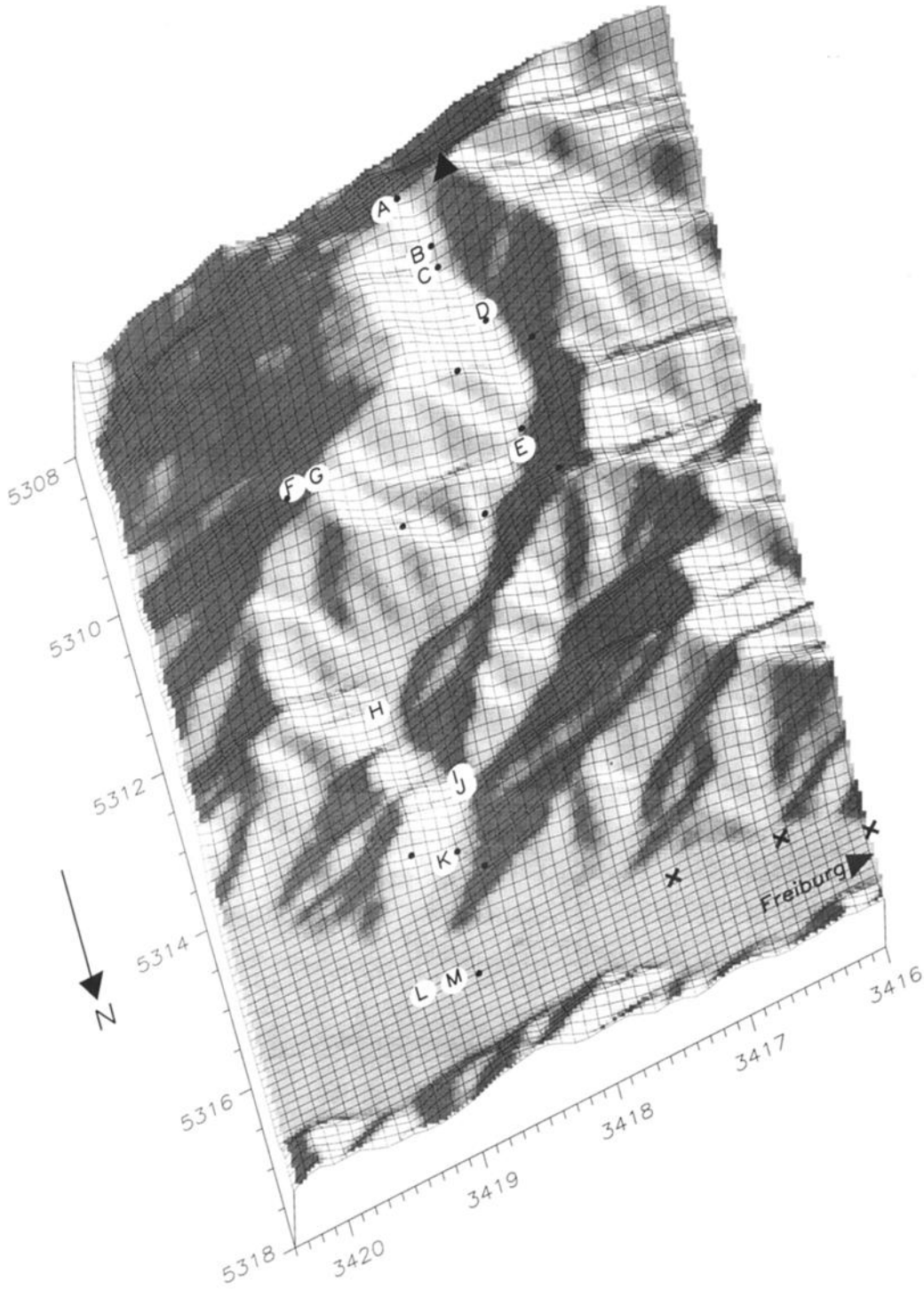

Figure 1. Map of the area between Freiburg and Schauinsland with the locations of the measurement sites in the Zarten Basin and the valley Großes Tal (see Table 1 for explanation). The Schauinsland summit is marked by a triangle. The chemical surface sites were located at point A (Schauinsland) and point K (Kappel).

of tropospheric carbon monoxide, submitted to *Journal of Geophysical Research*, 1999, hereinafter referred to as Holloway et al., submitted manuscript, 1999).

2.1.3. NO_x and NO_y. NO and NO_2 were measured at Schauinsland with two chemiluminescence detectors (CLDs) (ECO-Physics CLD 770 Al ppt) in combination with a photolytic converter (PLC) (ECO-Physics PLC 760). The instruments, which were developed and produced under license of FZJ, were improved by implementing a gold-plated reaction chamber. In order to avoid interferences from thermal decomposition of PAN, HO_2NO_2, etc., the power supply was removed from the housing of the PLC, and the photolysis cell was cooled by forced air.

NO_y was converted to NO on a gold tube (AuC) at 300°C in the presence of 0.1% CO [*Fahey et al.*, 1985] and measured by another CLD (same model). The converter was situated di-

Table 2. Instrumentation of the Chemical Surface Sites Schauinsland (SL) and Kappel (K1)

Parameter	Schauinsland (SL)	Time Resolution, min	Kappel (K1)	Time Resolution, min
Nitrogen monoxide (NO)	CLD770AL ppt (Eco Physics)	1		
NO + NO_2 (NO_x)	CLD770AL ppt (Eco Physics) with photolytic converter (PLC 760)	1	TE 42S (Thermo Environmental Instruments Inc.) with wet denuder and Mo converter	1
Odd nitrogen (NO_y)	CLD770AL ppt (Eco Physics) with gold converter	1	TE 42S (Thermo Env. Instr. Inc.) with gold converter	1
Water insoluble NO_y (NO_{yu})	CLD770AL ppt (Eco Physics) with wet denuder and gold converter	1		
Ozone (O_3)	TE 49 (Thermo Instruments)	1	TE 49 (Thermo Env. Instr. Inc.)	1
Carbon monoxide (CO)	TE 48 (Thermo Instruments)	1	TE 48 (Thermo Env. Instr. Inc.)	1
Hydrocarbons (C_2-C_6)	Sichromat 2-8 (Siemens) with cryogenic enrichment	90	HP5890 (Hewlett-Packard) with cryogenic enrichment	90
Hydrocarbons (C_6-C_7)	HC1010 (Airmotec)	20	HC1010 (Airmotec)	20
Biogenic hydrocarbons	GC-MS, Varian (Star 3400 Cx, Saturn 4D)	180	GC-MS, Varian (Star 3400 Cx, Saturn 4D)	180
Peroxiacetylnitrate (PAN)	PAN-GC (Meteorologie Consult)	10	PAN-GC (Meteorologie Consult)	10
Formaldehyde (HCHO)	AL4001 (Aerolaser)	1	TDL	1–2
Aldehydes (C_1-C_5)	DNPH and HPLC	30	DNPH and HPLC	30
NO_2 photolysis frequency (J_{NO_2})	filter radiometer (Meteorologie Consult)	1	filter radiometer (Meteorologie Consult)	1
O_3 photolysis frequency (JO^1D)	spectral radiometer (Meteorologie Consult)	4		
Global radiation	Pyranometer (Kipp&Zonen)	1		
Condensation nuclei	TSI model 3022	1		
Temperature	PT100 (Thies)	1	PT100 (Thies)	1
Wet temperature	PT100 (Thies)	1	PT100 (Thies)	1
Wind direction and speed	wind vane (Thies)	1	ultrasonic anemometer	1

rectly at the manifold. Another AuC/CLD combination was operated with a wetted denuder for the measurement of the unsoluble NO_y compounds (henceforth denoted NO_{yu}). The denuder consisted of a stripping coil (2 mm ID, 2 m long), similar to those used for H_2O_2 analysis [*Lazrus et al.*, 1986], which was fed with a flow of 0.03 mL/min of pure H_2O from a Milli-Q system and was kept at 10°C to avoid condensation of water vapor in the tubing behind the denuder. The use of four individual CLDs in combination with the different converters provided simultaneous measurements of NO, NO_x, NO_y, and NO_{yu}.

At Kappel, NO, NO_x and NO_y were measured with two commercial CLDs (Thermo Environmental Instruments Inc., Model TE 42S). The NO_y instrument was fitted with a self-built gold converter, which was installed at the inlet. For the measurement of NO_x the built-in Mo converter (MoC) of the TE-42S was used. The MoC is known to convert other NO_y compounds in addition to NO_2 [cf. *Fehsenfeld et al.*, 1987]. The major interference in the polluted planetary boundary layer (PBL) is peroxyacetic nitric anhydride (PAN), which is quantitatively converted to NO, and HNO_3, an unknown fraction of which is converted by the MoC. Therefore a bubbler filled with pure water was installed in the inlet line, in order to quantitatively remove HNO_3 (and other soluble NO_y compounds) before the sample entered the MoC of the NO_x instrument. PAN, which was measured separately (see below), was subtracted during data reduction.

At both sites the CLDs were calibrated daily by adding a small, known flow of a calibration gas (nominally 10 ppm NO in N_2, British Oxygen Corp.) into the ambient airstream at the inlet. The dilution factor was derived from the measured flow rates. The resulting NO mixing ratios in the sampled air were of the order of 10–50 ppb. The NO mixing ratio in the calibration gas was determined by gas phase titration with O_3 and can be traced to a calibrated O_3 monitor. A comparison with the NO standard of the NOAA Aeronomy Laboratory showed deviations of <2% [*Gerbig et al.*, 1996]. Losses of NO in the inlet system due to reaction with ambient O_3 (4% for 100 ppb O_3) were quantified by comparison with additional calibrations using synthetic air as dilutant.

The conversion efficiencies of the PLC and the AuC for NO_2 were determined on a daily basis with NO_2 obtained by gas phase titration of the NO standard. The NO calibration gas was mixed with O_3 produced by irradiation of O_2 at 185 nm (Hg lamp) in a flow of 20 mL/min and passed through a glass volume large enough that the O_3 was quantitatively converted (>99.5%). The Hg lamp was adjusted such that 70–80% of the NO were converted to NO_2. Calibrations with zero air were made every day for determination of the instruments' background, which was <10 ppt for NO and NO_2, 300 ± 100 ppt for NO_y, and 150 ± 80 ppt for NO_{yu}. The NO_y and NO_{yu} data were corrected accordingly.

The conversion efficiency of the PLC depends on the ambient concentrations of O_3 and NO_x. This is taken into account by solving numerically a simple time-dependent photochemical model of the PLC (reactions (R1) and (R2)).

$$\text{(R1)} \qquad NO_2 + h\nu + O_2 \rightarrow NO + O_3$$

$$\text{(R2)} \qquad NO + O_3 \rightarrow NO_2 + O_2$$

Under the assumption of mass conservation the three equations

$$d[NO]/dt = d[O_3]/dt = -d[NO_2]/dt$$

$$= [NO_2] \times J'_{NO_2} - [NO] \times [O_3] \times k_2 \qquad (1)$$

are integrated over the residence time of the air in the photolysis cell, t_R = 10 s. Here k_2 is the rate coefficient for the

reaction of NO with O_3 (reaction (R2), with $k_2 = 2.0 \times 10^{-12} \exp(-1400/T)$ [*DeMore et al.*, 1997]), and J'_{NO_2} is the photolysis frequency of NO_2 in the photolysis cell, which is determined during calibration (see below). The initial conditions $[NO]_o$ and $[O_3]_o$, that is, the ambient NO and O_3 concentrations, are taken from the simultaneous measurements. The third initial condition, the unknown ambient NO_2 concentration $[NO_2]_o$, is found in an iterative procedure: The first guess for $[NO_2]_o$ is based upon Leighton's ratio [*Leighton*, 1961]; that is, $[NO_2]_o = [NO]_o \times [O_3]_o \times k_2/J'_{NO_2}$. Equation (1) is then integrated and yields a value for $[NO]_{tR} = [NO]_o + \int (d[NO]/dt)\, dt$, the expected NO concentration downstream of the photolysis cell. Subsequently, the value for $[NO_2]_o$ is altered until the deviation of the calculated $[NO]_{tR}$ from the measured NO concentration behind the PLC becomes smaller than 0.1%.

A similar numerical model is used to evaluate the calibration data. The value for the photolysis frequency of NO_2 in the photolysis cell (J'_{NO_2}) is altered until the model calculates the correct value for $[NO]_{tR}$ from the known initial concentrations $[NO]_o$, $[O_3]_o$, and $[NO_2]_o$.

The conversion efficiency of the NO_y converters was determined at random intervals with HNO_3 from permeation tubes, in addition to the daily calibration with NO_2. The permeation tubes consisted of a 1/16 inch OD PFA tubes immersed into a mixture of concentrated H_2SO_4 (65%) and HNO_3 (35%). The solution was thermostatted at 30°C, and the PFA tube was continuously purged with zero air at a flow rate of 10 mL/min. The permeation rate was determined as follows: After each calibration, the HNO_3 was quantitatively (>99%) absorbed in a known amount of water, and the resulting NO_3^- concentration in the samples was measured after the campaign at the central analytical laboratory of Forschungszentrum Jülich (FZJ) by ion chromatography versus a $NaNO_3$ standard solution. From measurements behind the denuder used for absorption of the HNO_3 and by measurements with Luminol chemiluminescence (LMA-3, Scintrex), it was shown that the HNO_3 permeation tube produces only a small fraction of odd nitrogen in the form of NO_x (NO < 1% and NO_2 < 5% of HNO_3). Interference tests that were made prior to SLOPE96 showed that the gold converter did not significantly convert acetonitrile under the operating conditions employed.

At SL the detection limit (2 sigma) for an integration time of 10 min was 20 parts per trillion by volume (pptv) for NO, 40 pptv for NO_2, 200 ppt for NO_y, and 100 pptv for NO_{yu}. The precision (1 sigma at 20 ppb) as estimated from the reproducibility of the calibrations was 2% (NO), 4% (NO_2), and 3% (NO_y and NO_{yu}), respectively. At K1 the precision was similar, and the detection limit was 150 ppt for NO, 180 ppt for NO_2, and 200 ppt for NO_y. For the accuracy of the measurements, another 5% uncertainty associated with the NO calibration gas must be added.

2.1.4. PAN. Peroxyacetic nitric anhydride (PAN) was measured at both sites with automatic capillary gas chromatographs (GCs) (Meteorologieconsult GmbH, PAN-Analyzer) equipped with electron capture detectors. The systems had a detection limit (2 sigma) of 50 ppt and provided a measurement every 10 min. Calibration of the PAN-GCs was made by generating PAN in situ from the NO calibration gas via photolysis of acetone. The NO calibration gas is mixed with a flow of zero air containing several 100 ppm of acetone, which is added to the airflow by means of a permeation device. The mixture is then irradiated at 250 nm in a photolysis cell (residence time 5 min). The acetylperoxy radicals from the photolysis of acetone first oxidize the NO to NO_2 and then combine with the NO_2 to form PAN. According to model simulations of the system, methyl nitrate is the only significant by-product (<5% of PAN). It is formed from the CH_3 radicals formed in the photolysis of acetone. During extensive tests of the calibration unit that were carried out by us as part of the quality assurance program of the German Tropospheric Research Focus (TFS), the calibration unit was found to convert NO to PAN with a stoichiometry of 90 ± 5% (2 sigma) with CH_3ONO_2 being the only significant by-product (for more details, see *Volz-Thomas et al.* [1998]). A comparison of the two PAN calibration units during SLOPE96 showed agreement within 1%.

2.1.5. Carbonyl compounds. Measurements of formaldehyde (HCHO) were performed during the intensive observational periods (IOP) of SLOPE96, using three different techniques. In situ measurements were made at K1 with a homebuilt Tunable Diode Laser Absorption Spectrometer (TDLAS) [*Klemp et al.*, 1994; *Kern et al.*, 1996] and at SL with a commercial Hantzsch monitor (Aero-Laser, AL 4001). Discontinuous analyses of HCHO and other carbonyl compounds (CH_3CHO, CH_3COCH_3, and higher homologues) were made at both sites with the dinitro phenylhydrazine (DNPH) method [*Slemr et al.*, 1996]. In addition, a large number of higher carbonyl compounds were identified and quantified in samples analyzed for volatile organic compounds by GC-MS (see B. Kolahgar et al., unpublished manuscript, 1999).

The DNPH method utilizes sampling/derivatization on silica gel cartridges coated with dinitro phenylhydrazine (DNPH), followed by HPLC analysis of the hydrazones after elution from the cartridges. Sampling occurred for 40 min at a constant flow rate of 2 L/min. A potassium iodide filter upstream of the DNPH cartridge was used to destroy ozone during sampling. Determination of artifacts was done via blank samples which were handled as the air samples. The HPLC analysis was performed immediately after the IOPs. The reproducibility of the HPLC analysis was about ±3%. Calibration was performed by adding an internal standard to each sample (reproducibility ±3%), and the sampling efficiency was determined as >96% using certified permeation sources [*Slemr*, 1991]. Including uncertainties in the sample volume (±5%), the overall uncertainty of the technique is estimated to be less than 15% under laboratory conditions [*Slemr et al.*, 1996]. The detection limit for formaldehyde was 0.25 ppb, mainly caused by the magnitude of the blank.

The TDLAS detects HCHO by its absorption at about 1700 cm^{-1} in a 1 m multipath absorption cell (total light path: 100 m). The diode laser (Laser Photonics, 3256-09, liquid nitrogen cooled) is scanned over one rotational line of HCHO at a frequency of 15 Hz, and 900 scans are averaged for calculating 60 s averages (2-f-detection technique, modulation frequency 12.5 kHz). The pressure in the absorption cell is 50 mbar, and the flow rate of the sampled air is 6.6 L min^{-1} (STP). Before the campaign, the instrument was tested for interference from other species on the selected absorption line. The instrumental background was determined every 10 min by adding N_2 to the inlet instead of ambient air. Calibrations were made every 30 min by adding a reproducible flow of HCHO from a thermostatted permeation device to the N_2 flow at the inlet. Absolute calibration of the permeation device was performed both gravimetrically and colorimetrically using the chromotropic acid method [*Harris et al.*, 1989]. The detection

Table 3. Spectroscopic Data Used for the Calculation of Photolysis Frequencies

J_{ik}	Process	$\sigma_i(\lambda)$	$\phi_i(\lambda)$
J_{NO_2}	$NO_2 + h\nu \rightarrow NO + O(^3P)$	*Davidson et al.* [1988]	*Gardner et al.* [1987]
J_{O^1D}	$O_3 + h\nu \rightarrow O_2 + O(^1D)$	*Molina and Molina* [1986]	*Michelsen et al.* [1994]
$J_{H_2O_2}$	$H_2O_2 + h\nu \rightarrow 2OH$	*DeMore et al.* [1994]	yield = 1
J_{HONO}	$HONO + h\nu \rightarrow OH + NO$	*DeMore et al.* [1994]	yield = 1
J_{HCHO-a}	$HCHO + h\nu \rightarrow H + HCO$	*Moortgart et al.* [1983]	*Moortgart et al.* [1983]
J_{HCHO-b}	$HCHO + h\nu \rightarrow H_2 + CO$	*Moortgart et al.* [1983]	*Moortgart et al.* [1983]
J_{NO_3-a}	$NO_3 + h\nu \rightarrow NO + O_2$	*DeMore et al.* [1994]	yield = 1
J_{NO_3-b}	$NO_3 + h\nu \rightarrow NO_2 + O(^3P)$	*DeMore et al.* [1994]	yield = 1

limit, as estimated periodically from the differences between successive background spectra, was 0.25–0.3 ppb for a sampling interval of 1 min. It is limited by slow changes in the background spectra, mainly due to thermally induced changes in the laser alignment. An overall uncertainty of 15–20% is estimated from the uncertainties in the mass flows, the output of the permeation device, the errors due to fluctuations in laser intensity, and the errors introduced by the fit routine [*Kern et al.*, 1995].

The Aero Laser instrument is based on the Hantzsch reaction, that is, detection of the fluorescence (excitation 400 nm, fluorescence around 510 nm) of 3,5 diacetyl-1,4-dihydrolutudin which is formed in the reaction of formaldehyde with acetylacetone and NH_3 [*Dasgupta et al.*, 1988]. Quantitative transfer of HCHO into the liquid phase is achieved in a stripping coil. During SLOPE96 the instrument's background was determined 4–5 times per day by passing the ambient air over a hopcalite scrubber. The stability of the calibration was checked regularly by adding the internal permeation device to the zero gas stream. Absolute calibration was performed every day with a series of liquid standards ($(2 \times 10^{-8} - 5 \times 10^{-7})$ M), which were connected instead of the stripping solution. The detection limit was about 0.2 ppb. At concentrations >1 ppb the precision of the whole system as estimated from the calibrations was better than 15%.

2.1.6. Photolysis frequencies. The photolysis frequency of NO_2 (J_{NO_2}) was quantified in Kappel and at Schauinsland by measuring the UV actinic flux with two (upward and downward facing) 2π steradian filter radiometers (Meteorologie Consult GmbH). An assessment of the instrument and the measurement uncertainties is given by *Volz-Thomas et al.* [1996]. The radiometers were calibrated for J_{NO_2} with a chemical actinometer in Jülich (estimated accuracy 5% [*Volz-Thomas et al.*, 1996]). A recent comparison with the chemical actinometer of F. Rohrer and D. Brüning (manuscript in preparation, 1999) showed agreement within 4%.

During the IOPs a spectroradiometer (Meteorologie Consult GmbH, Glashütten, hereinafter denoted SR) was deployed at Schauinsland for the measurement of photolysis frequencies. The instrument uses the same 2π steradian scattering head as the J_{NO_2} sensors. The scattering head is coupled to a scanning double monochromator (CVI Laser Corp., Model CM112, 2400 lines/mm grating, resolution: 1.0 nm) by means of a multimode quartz fiber bundle. Light detection occurs by a photomultiplier (Hamamatsu, R 759). Monochromator and photomultiplier tube (PMT) are mounted in a hermetically sealed and thermostatted housing, which is pressurized with N_2. The spectra are scanned at a rate of 0.5 to 1.4 nm/s, thus providing one scan every 113 s. The raw signals are stored on disc for further processing.

The photolysis frequency J_{ik} for a certain photolytic reaction k occurring upon absorption of a photon by a molecule i is calculated from the actinic flux and the spectroscopic data (absorption cross section $\sigma_i(\lambda)$ and quantum yield $\Phi_k(\lambda)$) according to [cf. *Madronich*, 1987]

$$J_{ik} = \int (F_a(\lambda) \times \sigma_i(\lambda) \times \Phi_k(\lambda))\, d\lambda \qquad (2)$$

The references for the molecular absorption spectra and quantum yields used in this study are summarized in Table 3. Calibration of the SR is performed in two steps: First, the relative spectral sensitivity of the instrument is calibrated with a certified Tungsten lamp (Osram, Model 64632, 100 W), which is placed in front of the 2π scattering dome. Then we integrate the normalized SR signal over the actinic interval of NO_2 and apply the J_{NO_2} value that is concurrently measured by the filter radiometer as a calibration factor. Subsequently, calibration factors were averaged over 1 day. Relative calibration was checked every day. At the same time, the calibration of the wavelength scale of the monochromator was calibrated using three lines of a low-pressure Hg lamp (296.5, 365.5, and 404.7 nm; accuracy ±0.1 nm), in addition to regular wavelength calibrations using Fraunhofer lines. The accuracy of the actinic flux measurement with the SR as estimated from the accuracy of the relative calibration (<4% over the wavelength range used) and the J_{NO_2} measurement (7%) is better than 10%.

With a stronger light source the tungsten lamp can be used to derive absolute calibration factors with an accuracy of 6% [*Hofzumahaus et al.*, 1999]. However, the procedure requires a stronger lamp and is technically difficult to conduct in the field with a 2π scattering dome, as the lamp must be placed very accurately at two distances.

2.1.7. Meteorological data. In addition to the extensive meteorological measurements described by *Kalthoff et al.* [this issue], wind speed and direction were measured by two-dimensional (2-D) ultrasonic anemometer (Siggelkow, ULLA) in Kappel and with a standard wind vane/three-cup anemometer at the TOR station. Pressure, temperature, and relative humidity were determined with Thies pressure sensors and aspirated psychrometers. The meteorological instruments and the radiometers were mounted at the same height as the inlets for the chemical measurements. The data of all instruments were recorded at a frequency of 1 Hz and then averaged over 1 min.

2.2. Airborne Measurements

Airborne measurements were made by MetAir with a self-launching motor glider (Stemme S10; wing span 23 m; maximum takeoff weight 980 kg; payload 310 kg; speed 120–180

Table 4. Instrumentation of the Aircraft

Parameter	Instrument/Method	Range From ... To	Resolution Parameter/Time	Precision/ Accuracy	Calibration or Checks
Air temperature	Thermocouple (Meteolabor)	−50 ... 50°C	0.1°C/10 Hz	0.1/0.5°C	ice water/mercury
Dew point	dew point mirror (Meteolab)	−50 ... 50°C	0.1°C/4 s	0.1/0.5°C	psychrometer
Five pressures (one absolute, four different)	capacitive sensors (Keller Druckmesstechnik)	300 ... 1300; 0 ... 50 hPa	0.02 hPa/10 Hz	0.1/0.5 hPa	factory-calibrated
Flow angles	differences of pairs (left/right, top/bottom)	−20 ... 20°C	0.1°/0.1 s	0.1°/0.5°	wind residuals
True airspeed and	calculated (p, T, u)	10 ... 70 m/s	0.1 m/s/10 Hz	0.2/0.5 m/s	wind residuals
Pressure altitude	integrated (p, T, u)	0 ... 7000 m msl	1 m/4 s	3/10 m	mountain tops
Position (x, y, z)	GPS (Trimble TANS Vector)	worldwide	7 m/1 s	20/100 m*	fix points from map
Ground speed (vx, vy)		worldwide	0.1 m/s/1 Hz	0.1/0.5 m/s	statically at ground
Attitude angles (azimuth, pitch, and roll)		worldwide	0.1°/3 ... 10 Hz	0.1/0.5°	statically at ground
3-d-wind (x, y, z)	postflight processing from parameters above	0.5 ... 30 m/s	0.5 m/s/3 Hz	0.5/1.0 m/s	wind during maneuvers
NO_2	Luminol chemiluminescence (Scintrex LMA-3)	0.1 ... 200 ppb	0.01 ppb/1 s	0.1/1.0 ppb	calibration gas†
O_3 (slow)	UV absorption (PSI)	2 ppb ... 1 ppm	1 ppb/4 s	1/2 ppb	calibration gas†
O_3 (fast)‡	Eosin-Y chemiluminescence (Scintrex, LOZ)	1 ppb ... 1 ppm	0.1 ppb/10 Hz	10 ppb	against UV photometer
Speciated hydrocarbons (C_4 ... C_{10})	gaschromatograph (Airmotec HC-1010)	10 ppt ... 10 ppb	10 ppt/10 min	10 ppt/50 ppt or 20%	calibration gas

*Depending on operation mode of the U.S. military navigation satellites.
†Low-ppb calibration equipment of PSI, scanning an array of NO_2/O_3 concentrations to calibrate also the interference with ozone.
‡The signals of the two monitors are combined to get both fast and stable measurements, overlapping in the range between about 30 and 600 s (see text above).

km/h; and up to 5 hours endurance). The instruments are carried below the wings in specially designed compartments. The details of the instrumentation are listed in Table 4. More details about the aircraft and its present instrumentation are given by *Neininger et al.* [1999].

O_3 was measured redundantly by UV absorption and by chemiluminescence with eosin-y (Scintrex, LOZ-3). The UV instrument being rather slow (precision of 1 ppb reached in 30 s) provides an accurate, temperature- and pressure-corrected measurement, whereas the chemiluminescence instrument provides a fast time response but is subject to relatively large drifts. During data reduction the fast signal is quasi-continuously tied to the UV measurement, whereby an accurate and fast (4 s) ozone measurement is obtained. The UV photometer is calibrated against a NIST standard photometer at the Paul Scherrer Institut (PSI).

NO_2 was measured by chemiluminescence with luminol (Scintrex LMA-3). The instrument was calibrated before and after the campaign at PSI using gas phase titration of NO with O_3. The calibration procedure produces a two-dimensional array of NO_2 (0–10 ppb) and O_3 (0–150 ppb) mixing ratios and is also used to establish the necessary corrections for nonlinearity, pressure, temperature, and O_3 interference.

High-resolution wind measurements were obtained by using the Global Positioning System (GPS) for determination of the attitude angles (orientation of the aircraft along three axes) in combination with a five-hole pressure probe for measurement of the flow angles. Additional parameters are listed in Table 4. The in situ measurements of speciated hydrocarbons are described by B. Kolahgar et al. (unpublished manuscript, 1999).

2.3. Balloon Soundings

For the vertical soundings at Kohlengrund (KG) by IMK, the tethersonde (AIR, Model TS-3A-SPH) was used. The maximum height for the system is 1000 m above the surface. Dry and wet bulb temperatures are measured by two carefully matched thermistors mounted inside a radiation shield, similar to an Assmann psychrometer. Aspiration occurred by a small fan. Precision for both temperatures is 0.5 K. Pressure, which is used for calculation of the balloon's altitude, is measured by a capacitive sensor (AIR). Wind speed is measured by a three-cup anemometer, and wind direction is derived from a small electronically controlled compass (precision 5°), with the assumption that the aerodynamic balloon serves as a wind vane, which orients the sonde.

For ozone the fast surface chemiluminescence sonde (GFAS, Model OS-B-2) developed by *Güsten et al.* [1992] was used. It utilizes the chemiluminescent reaction of ozone with coumarin 47. The system is lightweight and provides a fast time response. The accuracy of the measurement relies on frequent calibrations against a reference instrument such as a UV photometer (Environment, Model O_3 41M 1). Calibrations of the sonde are carried out before and after each sounding.

The tethered balloon system used by IVD for the measurements at K2 consists of a 85 m^3 tethered balloon equipped with instruments for meteorological parameters (wind speed, wind direction, dry temperature, humidity, pressure) and for the concentrations of O_3 and NO_2. The parameters are transferred every 10 s to a ground station via a telemetry system. A complete description of the balloon system and the instrumentation is given by *Baumbach et al.* [1993].

The sensors for the measurement of meteorological parameters are similar to those used by IMK at KG. O_3 was measured with a modified ozone sonde AIR-OZ-3A-T, which is calibrated against a UV photometer (Dasibi 1008) before and after each sounding. NO_2 was measured with a Scintrex LMA3. Normally, the LMA3 is calibrated by diluting NO_2 calibration gases with zero air. The absolute NO_2 concentration in the calibration mixtures is determined by the Saltzman method

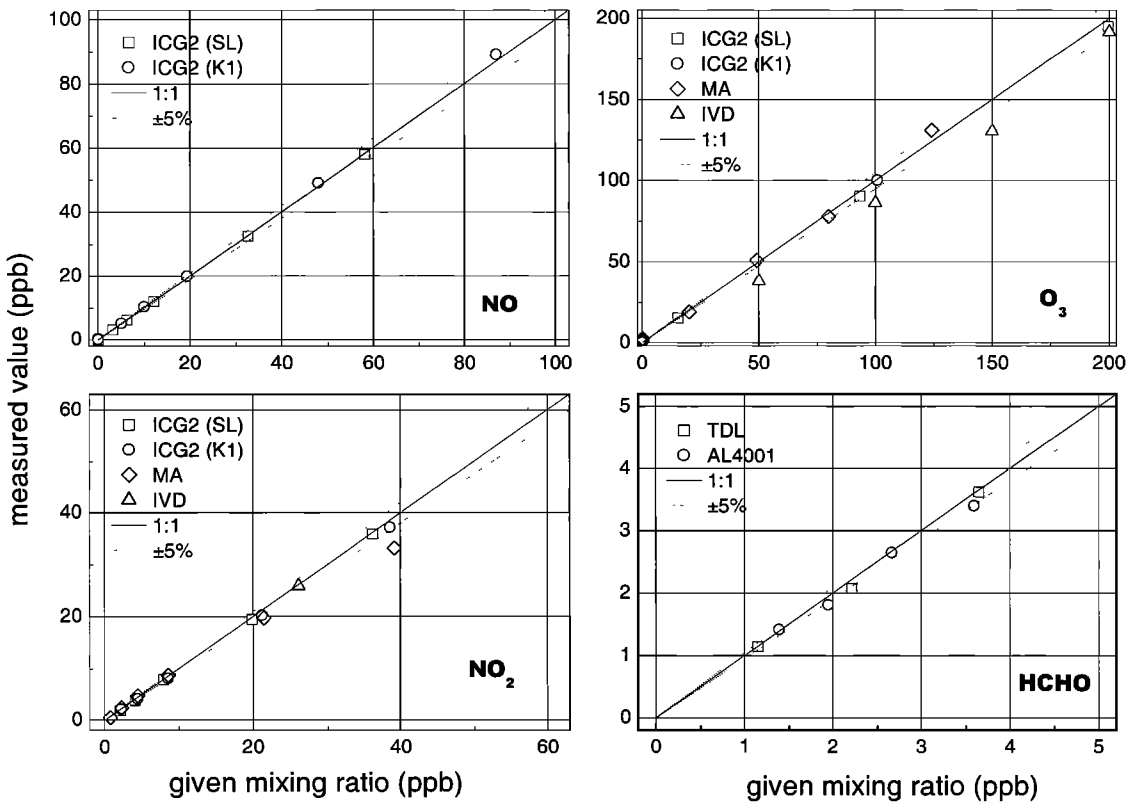

Figure 2. Intercalibration of O_3, NO, NO_2, and HCHO with reference gases (for acronyms, see Table 1).

[*Verein Deutscher Ingenieure (VDI)*, 1990]. During SLOPE96 the calibration system was found to be out of order. Therefore a standard mixture and dilution system of ICG2 was used during the campaign. Unfortunately, this system which had been designed for large concentrations and flow rates introduced significant errors in the lower ppb range, as is discussed below. For mixing ratios of several tens of ppb the dilution system of ICG2 was found to differ by less than 1% from the Saltzman method.

2.4. Instrument Comparison

An instrument comparison was organized in order to obtain information on the comparability of the different instruments deployed at the different field sites. The comparison was conducted in two steps: (1) a comparison of the calibration gases and calibration procedures was conducted before the campaign, and (2) concurrent measurements in ambient air were made after the first IOP. The comparison of the VOC measurements is discussed by B. Kolahgar et al. (unpublished manuscript, 1999).

For NO and NO_2, calibration gases from BOC (10 and 5 ppm, respectively) were diluted with zero air (Messer Griesheim) using a self-built multicapillary dilution unit. The flows were measured several times before, during, and after the experiments with an automatic soap film flowmeter (Gillian, Gillibrator). The uncertainty of the dilution factors, including possible errors in the humidity correction, was better than ±1%. The NO calibration gas was compared with the primary standard of ICG2, which had been compared to the standard used at the NOAA Aeronomy Laboratory (agreement better than 2% [*Gerbig et al.*, 1996]). For the comparison of O_3 a standard calibrator (TE 49PS) was used. The calibration gases were successively supplied to the inlets of the different instruments at ambient pressure and at excess flow. The comparison and data collection were conducted in a blind fashion by a person (A. Lerner) who was not otherwise involved in the campaign. The results were only revealed to the participants after all data had been supplied in final form.

The results of the comparison are shown in Figure 2 in the form of scatterplots of the measured values as reported by the different participants versus the theoretical concentrations, that is, those given by the calibrator in the case of O_3 and those calculated from the concentration in the calibration standards and the dilution factors in the cases of NO and NO_2.

In general, the agreement was within ±5%, except for the low-sensitivity commercial NO_x monitors of IMK and MIF (−15%, not shown), the data of which are not used in this paper because of the very large deviations found in ambient air. The LMA-3 of MetAir was in excellent agreement up to NO_2 mixing ratios of 10 ppb (i.e., the range over which it was calibrated). At higher mixing ratios the instrument tends to underpredict the NO_2 concentration (6% at 20 ppb and 10% at 40 ppb). The agreement of the instruments at the TOR station was within ±1%. The NO_2 calibration gas was also sampled and analyzed by IVD using the Saltzman method [*VDI*, 1990]. The results agreed with the predicted value within <1%.

For ozone the instruments agreed with the standard within ±3% (mostly within 2%), except for the highest value (120 ppb) where the deviation of the MetAir instrument was 5%. The UV absorption instrument (Dasibi 1008) used by IVD for calibration of their balloon sonde showed significantly lower values (−13%).

An independent HNO_3 permeation device was used for test-

ing of the conversion efficiency of the different converters employed for the measurement of NO_y. The HNO_3 source was characterized during the QA experiments by quantitative absorption of the effluent in water and quantification of the absorbed HNO_3 by measurement of the pH (in situ) and of the NO_3^- concentration (off-line by ion chromatography using a weighed $NaNO_3$ standard as reference). Both methods were found in agreement within 10%. The tests with the permeation tube showed that the gold converters used by ICG2 at SL and K1 converted HNO_3 with a conversion efficiency of >97%. Furthermore, it was shown that the bubbler used in front of the NO_x instrument in K1 indeed retained HNO_3 by >98%.

For the comparison in ambient air the instruments were gathered on June 7 at the mobile laboratory of ICG2 in K1. In order to facilitate the different instruments to measure the same air and to allow the possibility of spiking the ambient air with calibration gases, all NO_x instruments were connected to a common inlet that was put together from 1/2 inch OD PFA tubing. The ozone sondes being very sensitive to pressure changes were not connected to the common inlet line but were placed on the roof of the mobile laboratory with their inlets very close to the common inlet. The ozone sonde of IMK and the TE-49 of the TOR station SL, which had been compared before the campaign with the TE-49 of ICG2 in Kappel (agreement within 2%), did not participate in the comparison.

The results of the comparison are shown in Figure 3 as time series and in Figure 4 as scatterplots, using the instruments of the mobile lab as the reference. All three instruments reproduce the increase of O_3 between 2200 and 2300 hours, and most of the fine structure. The correlation between MIF and ICG2(K1) scatters around the 1:1 line with a standard deviation of ±1.3 ppb (±1.8%). The UV photometer of MetAir has a constant offset of about 3 ppb with respect to the TE-49 of ICG2. The ozone sonde of IVD gives systematically 15% lower values, quite similar to the findings with the calibration source. In order to harmonize all O_3 data obtained in SLOPE96 the results of IVD and MetAir were corrected on the basis of the results of the ambient comparison

$$\begin{aligned} \text{IVD} \quad & [O_3]_{cor} = [O_3] \times 1.2 - 5.9 \\ \text{MA} \quad & [O_3]_{cor} = [O_3] \times 1.02 - 4.9 \end{aligned} \tag{3}$$

The comparison for NO and NO_2 is also shown in Figures 3 and 4. In order to increase the dynamic range of the test and to obtain information on the time response of the instruments, the inlet line was spiked three times with NO_2 and twice with NO calibration gas, respectively. Because of the relatively long residence time in the common inlet line, a significant fraction of the NO was converted to NO_2 by reaction with ambient O_3. Because of the different residence times of the air in the inlet line for the different instruments, only the NO_2 spikes can be used reliably. The LMA-3 of MetAir gives systematically lower NO_2 concentrations than the TE-42S of ICG2 (−30% on average). A parabolic fit provides the best description of all data. The curvature is consistent with the results in Figure 2, where a similar underprediction is observed for the higher concentrations. The offset of −0.2 ppb is not significant. Good agreement over the range of ambient NO_2 (9–15 ppb) would be obtained when multiplying the MetAir data by a factor of 1.35. The reason for this large difference in response of the MetAir LMA-3 as compared to the results in Figure 4 was not resolved during SLOPE96. Recalibration of the instrument after the

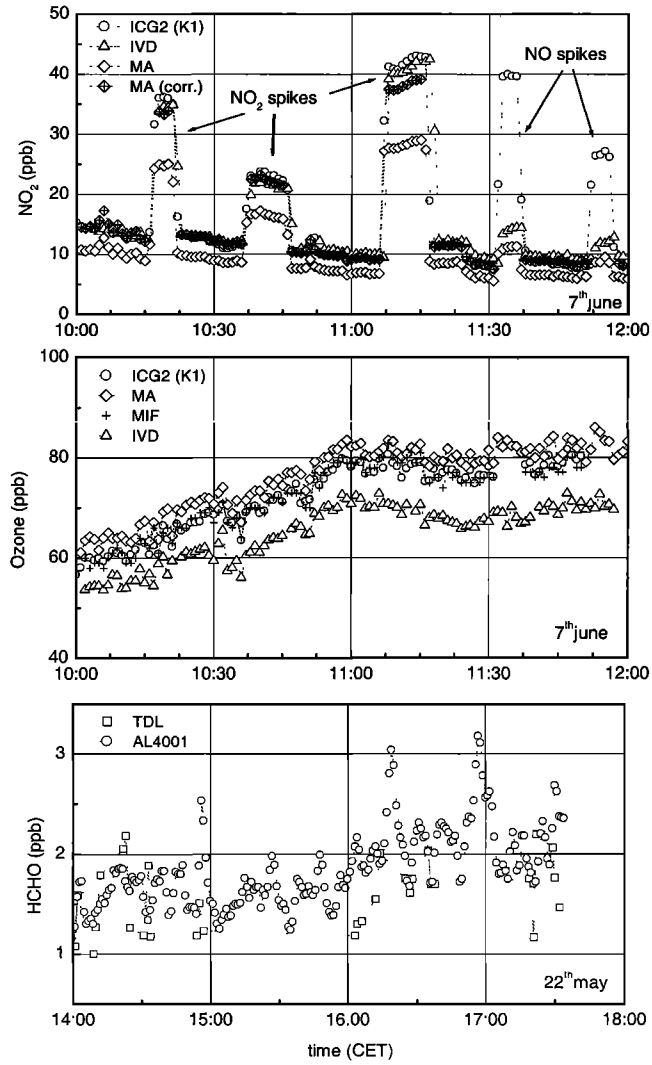

Figure 3. Time series of NO_2 and O_3 during the ambient instrument comparison on June 7. The inlet was spiked three times with NO_2 and two times with NO calibration gas. The lowest panel shows the HCHO measurements by the Hantzsch technique (Al4001) and TDLAS during the comparison on May 22. For acronyms, see Table 1.

campaign at PSI gave the same calibration coefficients as before. The most likely explanation was the temperature of the instrument housing exceeding 35°C during the ambient comparison. Although the housing was protected from direct insolation, it was not ventilated as it would be during flights, and the place on the roof of the mobile laboratory of ICG2 was hot. The known temperature dependence of the luminol chemiluminescence is electronically compensated in the LMA-3 and is further corrected during data reduction. However, this procedure is only reliable for temperatures below 30°C. Laboratory tests have shown that the degradation of the sensitivity escalates above 30°C. Since the recorded instrument temperature was always below 27°C during airborne operation and because of the good agreement found with the measurements made at Schauinsland (see below), we refrained from correcting the NO_2 data of MA.

The agreement between IVD and ICG2 is within 10% for both ambient concentrations and NO_2 spikes (average slope of

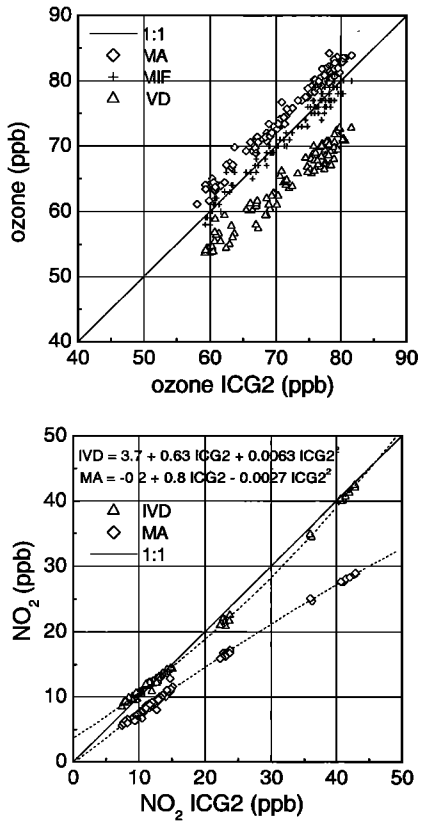

Figure 4. Scatterplots of the ambient measurements in Figure 3 (for acronyms, see Table 1). The NO spikes have been removed from the data.

all data 0.96), although the slope of the correlation for the ambient data seems to be significantly below unity (IVD/ICG2 = 0.9). A parabolic fit (dashed line) provides a better description of the entire data set but extrapolates to an offset of 3.7 ppb. After the campaign, it was found that significant NO_2 losses occurred in the dilution system of ICG2 that was used during SLOPE96 for calibration of the LMA3 of IVD. The relative losses increased with decreasing NO_2 concentration (<5% at 10 ppb and almost 100% below 0.5 ppb at a total flow of 2 SL min^{-1}).

In order to investigate the apparent discrepancies in the different NO_2 measurements the NO_2 data of MetAir were compared during the campaign with those from the surface station SL and from the tethered balloon of IVD, respectively. In situations when the aircraft flew within a box of $\pm 500 \times 500 \times 50$ m^3 (x, y, z) centered at SL, good agreement (within ± 0.2 ppb) was obtained for NO_2 mixing ratios in the range of 1–3 ppb. For ozone an offset of 3 ppb was found for the uncorrected data, slightly less than that observed during the instrument comparison (Figure 4).

The NO_2 mixing ratios by IVD were much larger than those measured by MetAir (up to a factor of 1.6 for NO_2 mixing ratios below 5 ppb). On the other hand, the data from IVD collected when the balloon was near the surface agreed fairly well (within 10%) with the measurement of the ground station in K1 during homogeneous situations with NO_2 mixing ratios around or greater than 10 ppb. These findings are in accordance with the erroneous behavior of the NO_2 calibration system used for IVD. Consequently, the IVD data were corrected according to

$$[NO_2]_{cor} = [NO_2] \times \{1 - \exp(-[NO_2]/3.5)\} \quad (4)$$

The magnitude of the correction decreases exponentially from −100% at 0 ppb to −10% at 10 ppb. The correction largely removes the slight curvature of the IVD/ICG2 correlation in Figure 4 and greatly reduces the discrepancies between IVD and MetAir, without changing the good agreement between IVD and ICG2 for the higher NO_2 mixing ratios.

In conclusion, the data from the ICG2 sites at Schauinsland and Kappel and the data from the aircraft and the tethered balloon agree within 10% or ±0.2 ppb after correction of the IVD data for calibration errors in the lower ppb range. Below 3 ppb the NO_2 data of IVD have a large uncertainty and should only be regarded as semiquantitative information. Above 6 ppb the data are comparable to the rest of the data set within 10–20%.

The last panel in Figure 2 shows the results of the HCHO measurements by TDLAS and the Hantzsch monitor at a calibration system consisting of a permeation source and a dilution unit (Kin-Tek). Both instruments had been calibrated before with their own calibration procedures as described above. Linear regressions for the two instruments give slopes and offsets of 1.0; 50 ppt for TDLAS and 0.93; 90 ppt for the AL4001. The maximum deviations for the different concentrations are <5%. The DNPH method did not participate in the intercomparison.

A comparison for HCHO in ambient air was conducted on May 22, a cloudy day with little photochemical activity. The results are shown in Figure 3. According to the Hantzsch monitor (Al4001), HCHO mixing ratios scattered around a mean value of 1.5 ppb for the first hour of the comparison and increased slightly to about 2 ppb thereafter. The two instruments were in reasonable agreement, with an average difference (Al4001-TDLAS) of 0.22 ppb.

The two filter radiometers for the measurement of J_{NO_2} were operated side by side at Schauinsland before the campaign. The agreement was better than 5%, similar to what was found during the calibration of the two sensors in August 1996 at Jülich.

3. Results

Figure 5 shows the concentrations of O_3, NO_y, CO, and meteorological parameters measured at SL for the entire period of the campaign. The SLOPE96 IOPs are marked with windows. As is described by *Volz-Thomas et al.* [this issue], the major goal of SLOPE96 was to study the chemical degradation of anthropogenic precursors and photooxidant formation in the plume of Freiburg during transport through the valley Großes Tal to Schauinsland. The long-term observations at Schauinsland had shown that the thermally driven wind system in the valley is established only at wind speeds <3 m/s. The most favorable meteorological condition is an anticyclone over Europe associated with weak southeasterly geostrophic flow over southwest Germany. On average, this situation occurs on about 30% of the days in summer [*Volz-Thomas et al.*, this issue]. The ideal situation is depicted by three features: Owing to the onset of the valley wind system, wind direction at SL changes in the morning from east or southeast to northwest, and wind speed remains below 3 m/s; the anthropogenic precursors, such as CO and NO_y, show a sharp increase and stay

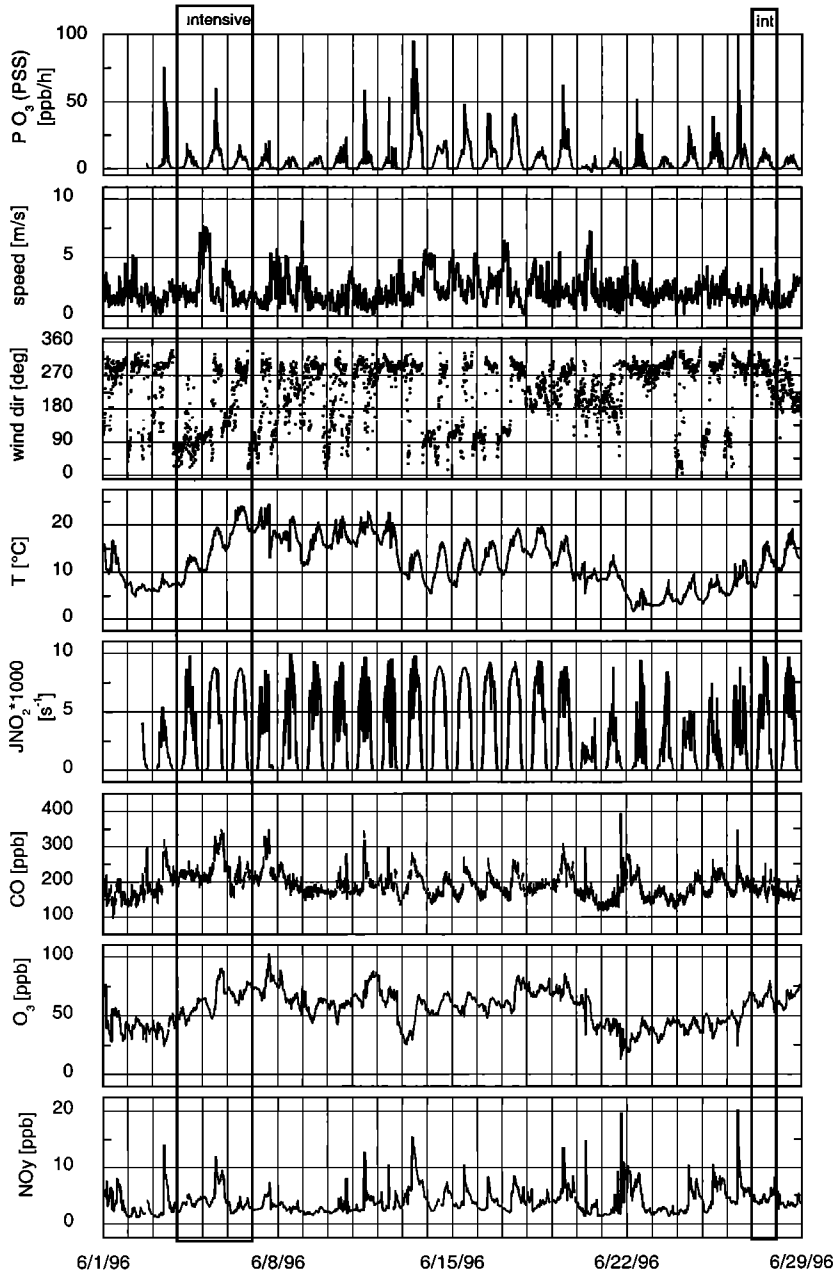

Figure 5. Mixing ratios of selected trace gases and meteorological parameters measured at the TOR station Schauinsland in June 1996. The boxes denote the intensive observational periods (IOP). The upper panel gives the ozone production rate as derived from PSS.

high for several hours; temperature and ozone increase together and reach their maximum values in the afternoon.

The meteorological situation during June 1996 was somewhat atypical with long periods of relatively strong northwesterly winds. Periods with fair weather were observed between June 4–6 and June 13–19 (see J_{NO_2} data in Figure 5). The valley wind system is seen in both periods. The first period was clearly identified in the forecast, and the first IOP was conducted between June 4 and 6. It will be discussed in more detail below. As is depicted by the wind data and the chemical species in Figure 5, June 13 would have been rather ideal with peak NO_y mixing ratios of 15 ppb. However, the necessary change in general circulation, as depicted by the change in wind direction to east, was very difficult to forecast and did not occur before the early morning of June 14, after a longer period of persistent northwesterly winds and after the passage of a front on the day before. Although the valley wind system is seen on the following 3 days in the wind data, the precursor concentrations remain rather low (CO hardly exceeds 250 ppb), and little ozone increase is observed over the period. The increase in temperature is also much less pronounced than during the first IOP.

The rest of the month was predominantly cloudy. A second IOP was called for June 27 and 28, the last 2 days of the fixed time window of SLOPE96. As the meteorological situation was less favorable than expected from the forecast and did not lead to a situation useful for studying photochemistry in the city plume of Freiburg, the campaign was ended on the evening of the June 27.

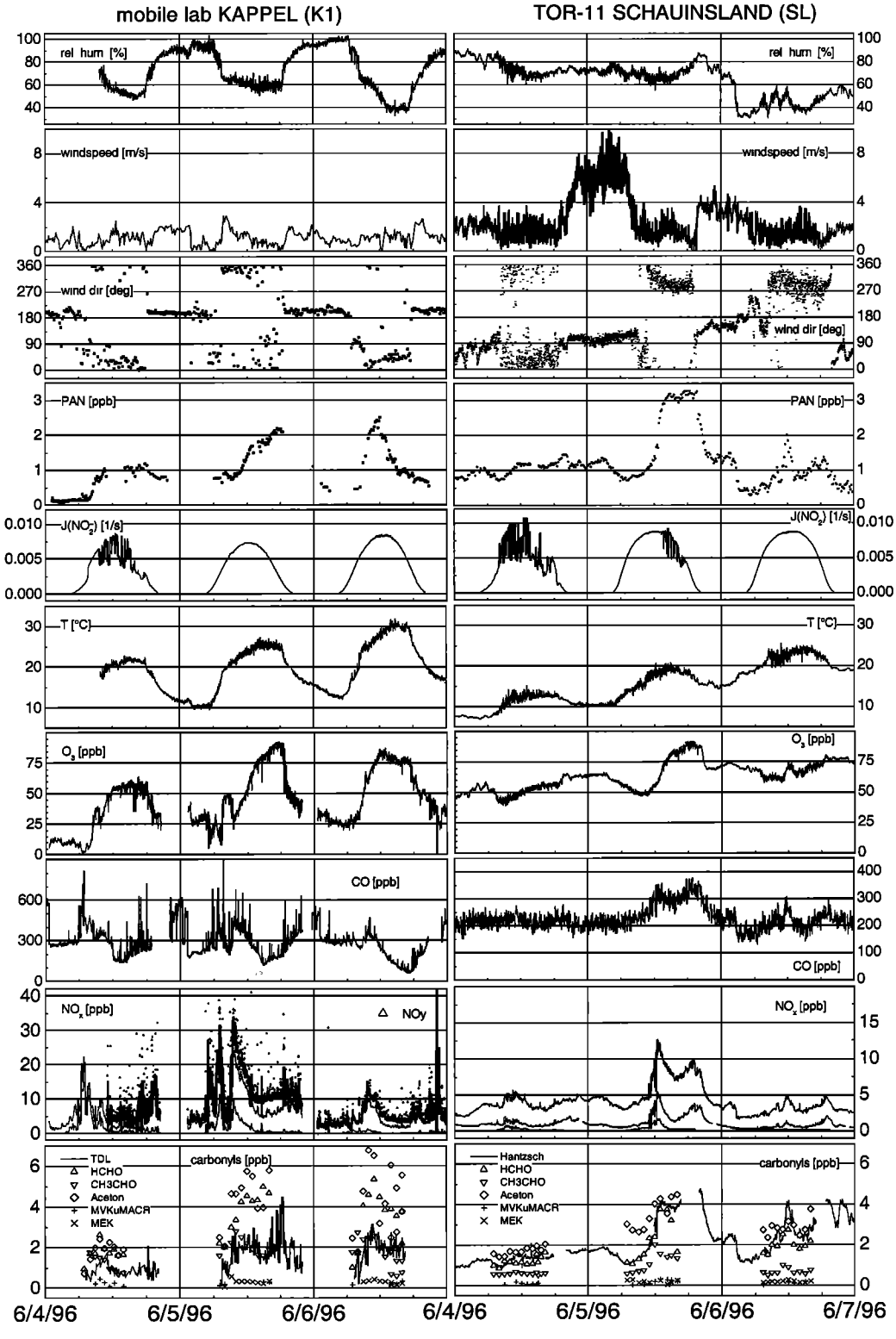

Figure 6. Mixing ratios of trace gases, J_{NO_2}, and meteorological parameters at SL and at K1 during the first IOP (June 4–6, 1996).

3.1. Ground-Based Measurements

Figure 6 shows the concentrations of all trace gases measured at K1 and at SL during the first IOP (June 4 to 6). The situation was dominated by easterly geostrophic winds, gradually changing from NE on June 4 to more southerly directions on the following days. From the wind data at K1 the valley wind system in the Großes Tal began to establish between 0700 and 0800 central European time (CET) and lasted until 1700 to 1800. In the data from SL the valley wind system is marked by the change to northerly directions. At Kappel the transport

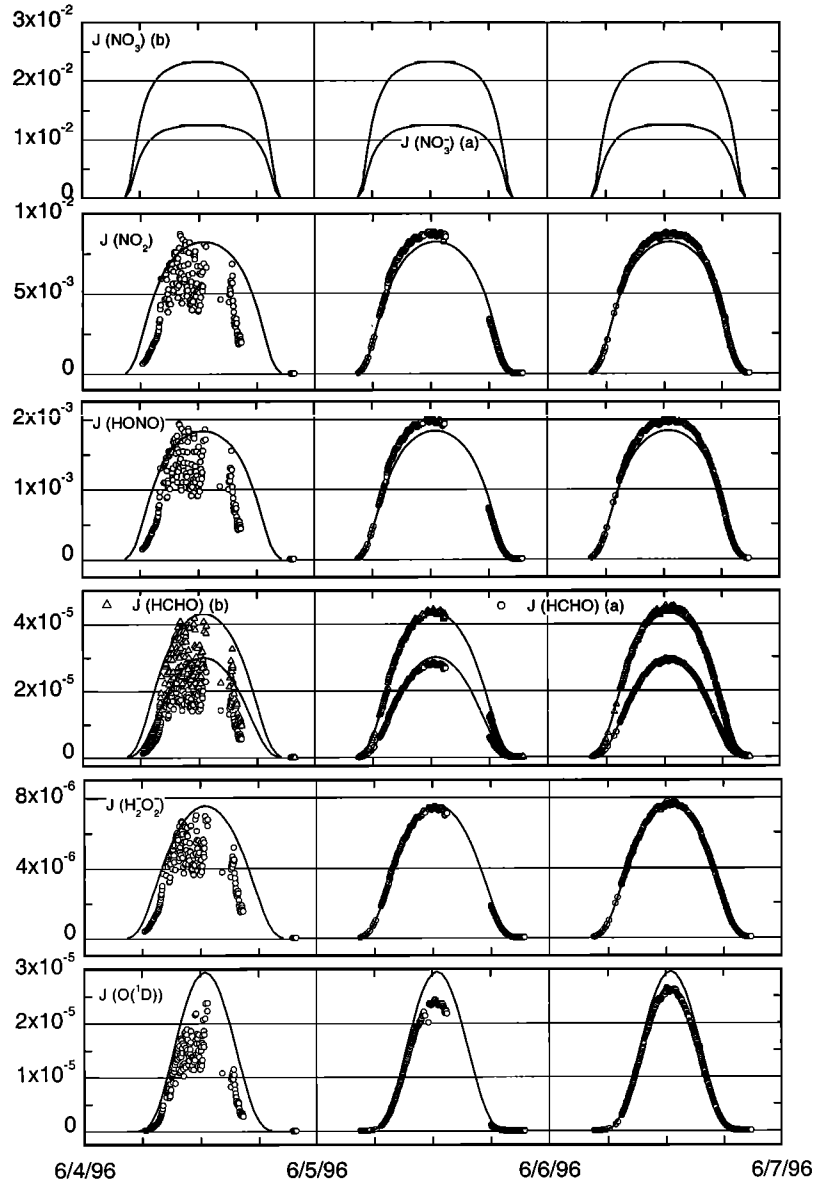

Figure 7. Photolysis frequencies of selected trace gases during the first IOP from the measurements with the spectroradiometer at Schauinsland (symbols). The gap in the afternoon of June 5 is due to a failure of the data recording system of the SR. The solid lines are model calculations with a discrete ordinate model (clear sky, 300 DU, 1250 m asl, surface at 1200 m asl).

of polluted air is seen on the first 2 days of the IOP. At Schauinsland, however, the advection of polluted air is most pronounced on June 5.

On June 4 the presence of scattered clouds is evident from the J_{NO_2} data. The concentrations of the anthropogenic precursors remained relatively low, and ozone mixing ratios did not exceed 60 ppb on that day. On June 5 the valley wind system was fully established at 0730 CET. The maximum mixing ratios of anthropogenic precursors (40 ppb for NO_x) are reached around 0930 CET at Kappel. The small maxima at 0500 and 0800 CET are due to advection from the Zarten Basin [see *Kalthoff et al.*, this issue], although contributions from local traffic during this period cannot be ruled out completely. At Schauinsland the maximum mixing ratio of NO_x (7 ppb) is reached at 1230 CET. However, as is discussed in more detail by *Kalthoff et al.* [this issue] and *Fiedler et al.* [this issue], the wind at Schauinsland had already turned toward more westerly directions, due to heating of the slopes of the Rhine valley. The valley wind system in the Großes Tal was only responsible for the first small maximum (4 ppb) in NO_x observed around 1120 CET at SL. This is also seen in the NO_2 data from the tethered balloon (Figure 8) and from the aircraft (Figure 10). On June 6, relatively low precursor concentrations are observed at Kappel. A possible explanation is that due to the bank holiday, the emissions occurred later in the day when vertical mixing was already more pronounced.

HCHO and the other carbonyl compounds are shown in the lowest panels of Figure 6. The DNPH method gives similar HCHO concentrations at both sites with maximum concentrations around 4 ppb. At SL the DNPH measurements are in reasonable agreement with the HCHO measurement by the Hantzsch technique, whereas the TDLAS at K1 measured al-

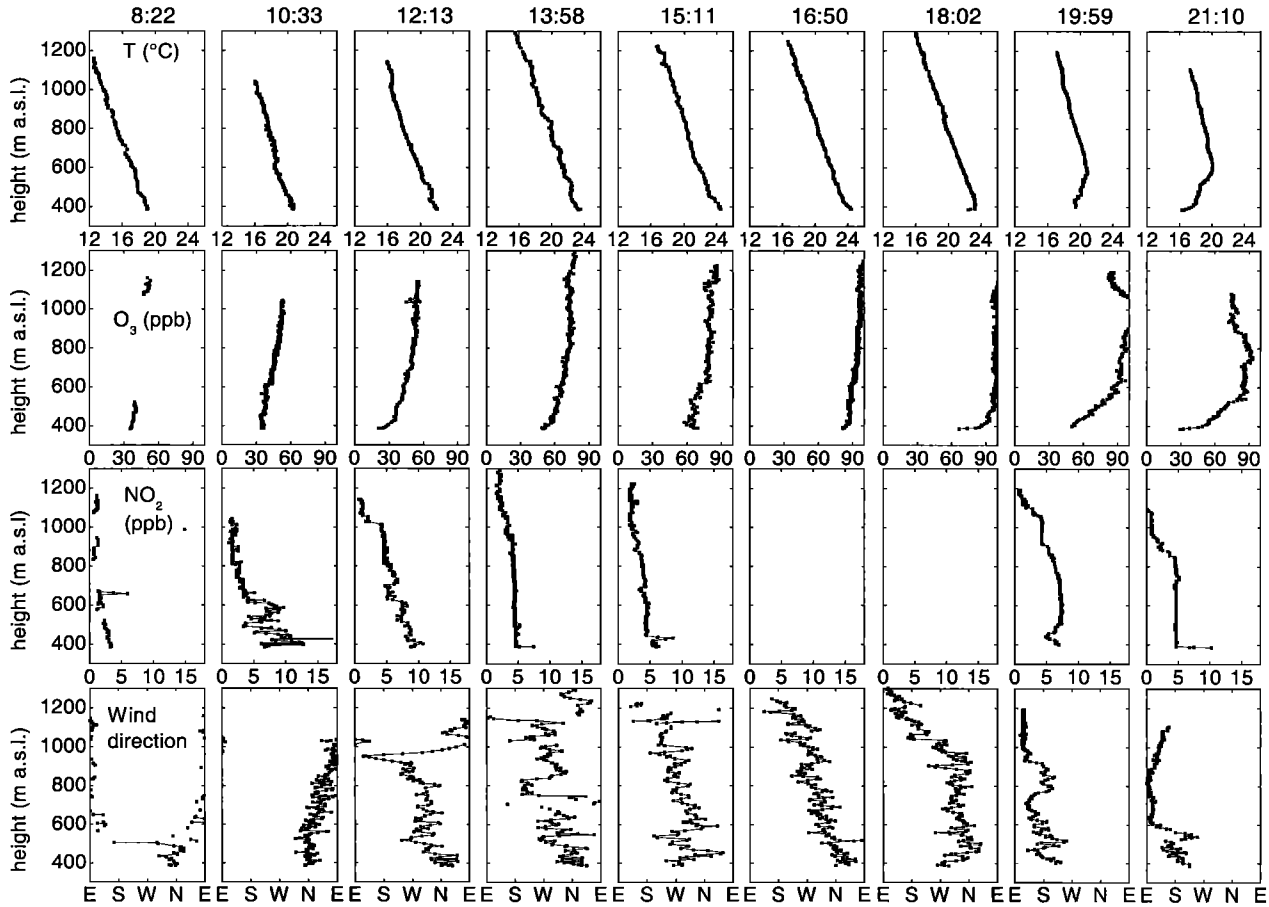

Figure 8. Vertical profiles of O_3, T, NO_2, and wind direction on June 5 at K2. The beginning of a sounding (CET) is denoted above the panels.

most a factor of 2 lower HCHO concentrations than the DNPH method. Obviously, HCHO is either underestimated by TDLAS, or interferences must exist with the other two techniques. This is puzzling because of the good agreement between TDLAS and Hantzsch monitor during the intercomparison and because a negative interference with TDLAS, a highly specific spectroscopic method, is difficult to imagine. The relatively good agreement observed during the instrument comparison in ambient air under cloudy conditions (<0.3 ppb, Figure 3) would suggest a potential interference being caused by a photochemically produced compound. Similar results were obtained during a field comparison in 1998, with relatively good agreement between AL4001 and TDLAS under cloudy conditions and a factor of 2 difference between the Al4001 and TDLAS, when polluted air was analyzed during intensive insolation (D. Klemp et al., manuscript in preparation, 1999). Until clarification is obtained, the HCHO mixing ratios measured at Schauinsland must be regarded as upper limits, and the TDLAS data from K1 must be regarded as lower limits.

Figure 7 shows the photolysis frequencies of different molecules as obtained from the spectroradiometer. Also shown are model calculations with the radiative transfer model of Madronich (discrete ordinate scheme of *Stamnes et al.* [1988]) for clear-sky conditions, using the same spectroscopic data as for the SR. The model predicts 5–10% lower values for J_{NO_2}, with which the SR is calibrated, except for the first day which was partially cloudy. The discrepancy is similar to the results obtained by *Volz-Thomas et al.* [1996] and within the uncertainty of the measurement. While the agreement is similar or better for HCHO, H_2O_2, and HONO, the model overestimates J_{O1D} by 15–20% with respect to the SR. This discrepancy is larger than the uncertainty in the relative spectral sensitivity of the SR (4%). As the ozone column used in the model (300 Dobson units (DU)) is in agreement with data from the Global Ozone Monitoring Experiment (GOME) instrument on ERS2 [*Burrows et al.*, 1999] for the period of the first IOP of SLOPE, we have no clue on the source for the discrepancy.

3.2. Balloon Soundings

The balloon data from K2 show results similar to the ground-based measurements at K1. On June 4 the northerly valley wind extended to approximately 200 m aboveground. Above, the wind direction changed to east. This situation lasted until the late afternoon. The balloon measurements indicated that no relevant transport of polluted air along the valley occurred.

Also on June 6 the valley wind system was unstable according to the measurements made by the tethered balloon at K2. In the morning hours the magnitude of the valley wind regime exhibited relatively large fluctuations between zero and about 400 m aboveground.

Figure 8 displays the results from vertical soundings made on June 5 at K2. Each row shows the vertical profiles of tem-

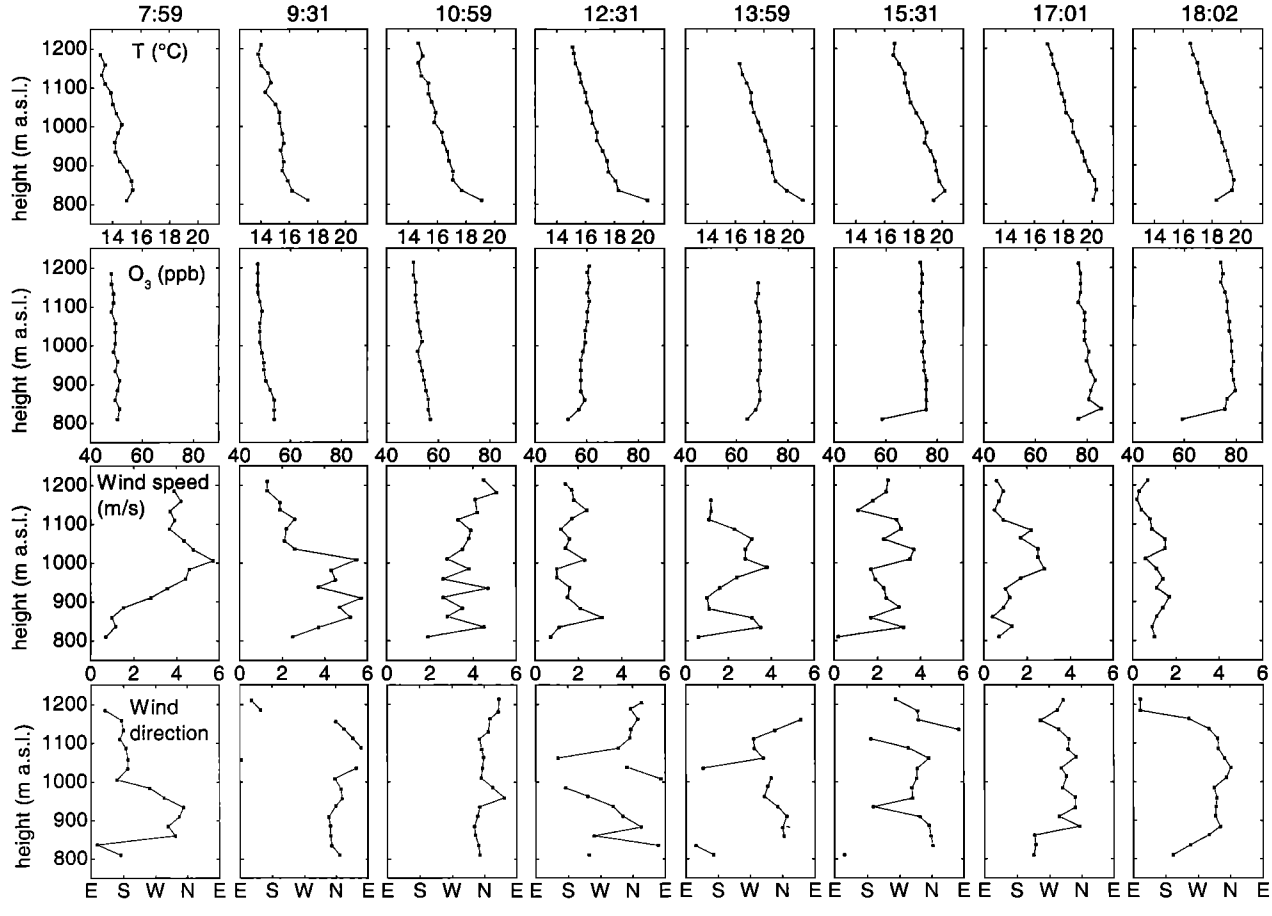

Figure 9. Vertical profiles of O_3, T, wind speed, and wind direction on June 5 at KG. The beginning of a sounding (CET) is denoted above the panels.

perature, ozone concentration, NO_2 concentration, and wind direction. It should be noted that the time required for a full ascent and descent is about 1 hour. Only the ascents are shown for clarity. During the first sounding (0822 hours), turbulent conditions prevailed near ground, whereas the geostrophic wind from easterly directions was observed at higher altitudes. In the sounding starting at 1033 hours the (northerly) valley wind is observed up to approximately 250 m aboveground. With increasing height the wind direction changes to east, indicating that the geostrophic wind is still dominant in levels of 500 m aboveground (900 m mean sea level (msl)) and higher. The northerly flow of the valley wind system is capped by an inversion layer, which efficiently inhibits vertical transport of air pollutants emitted near ground. NO_2, which characterizes the loading of the air mass with primary pollutants, shows a significant decrease from almost 10 ppb to about 3.5 ppb at 250 m aboveground, whereas O_3 increases by approximately 5 ppb. These profiles clearly show the transport of polluted air through the valley Großes Tal.

In the next sounding at 1213 hours the capping inversion has already climbed to 650 m (1050 m msl). The pollution is still trapped underneath, as can be seen from the strong gradient in the NO_2 mixing ratio at the altitude of the temperature inversion. In the subsequent soundings the capping inversion is not seen anymore and must therefore be above 1200 m (the maximum height of the balloon allowed at this site for air traffic security reasons). In the afternoon the profiles of the chemical species show little vertical gradients, indicating well mixed conditions in the boundary layer. The northerly flow persists only near the surface, whereas westerly winds are now observed at higher levels.

The later profiles exhibit the development of the nocturnal surface inversion. The wind direction at the surface has changed to south due to the mountain wind in the valley. The lack of increased NO_2 mixing ratios underneath the surface inversion proves the absence of significant nighttime pollution sources in the valley.

Figure 9 shows the vertical profiles of temperature T, ozone, wind speed, and wind direction obtained at Kohlengrund (KG). A shallow surface inversion of about 50 m thickness was still detectable at 0759 CET. Within this layer a weak southerly mountain wind of ~1 m s^{-1} existed. However, the surface observations indicated that shortly after 0800 CET the valley winds, that is, northerly winds, were established at KG [*Kalthoff et al.*, this issue].

By 0931 CET an unstable surface layer had developed, and the valley wind had extended up to ~1050 msl. The wind speed of the valley wind was at 4 to 5 m s^{-1} and dropped to around 2 m s^{-1} at the top of the valley wind regime. Ninety minutes later the top of the valley wind layer had risen to a height 1150 msl. At this altitude a slight turning of the wind from northerly to northeasterly directions was detected while the wind speed was still at 4 m s^{-1}. On the upper levels the valley wind system was later disturbed by regional-scale westerly winds. These

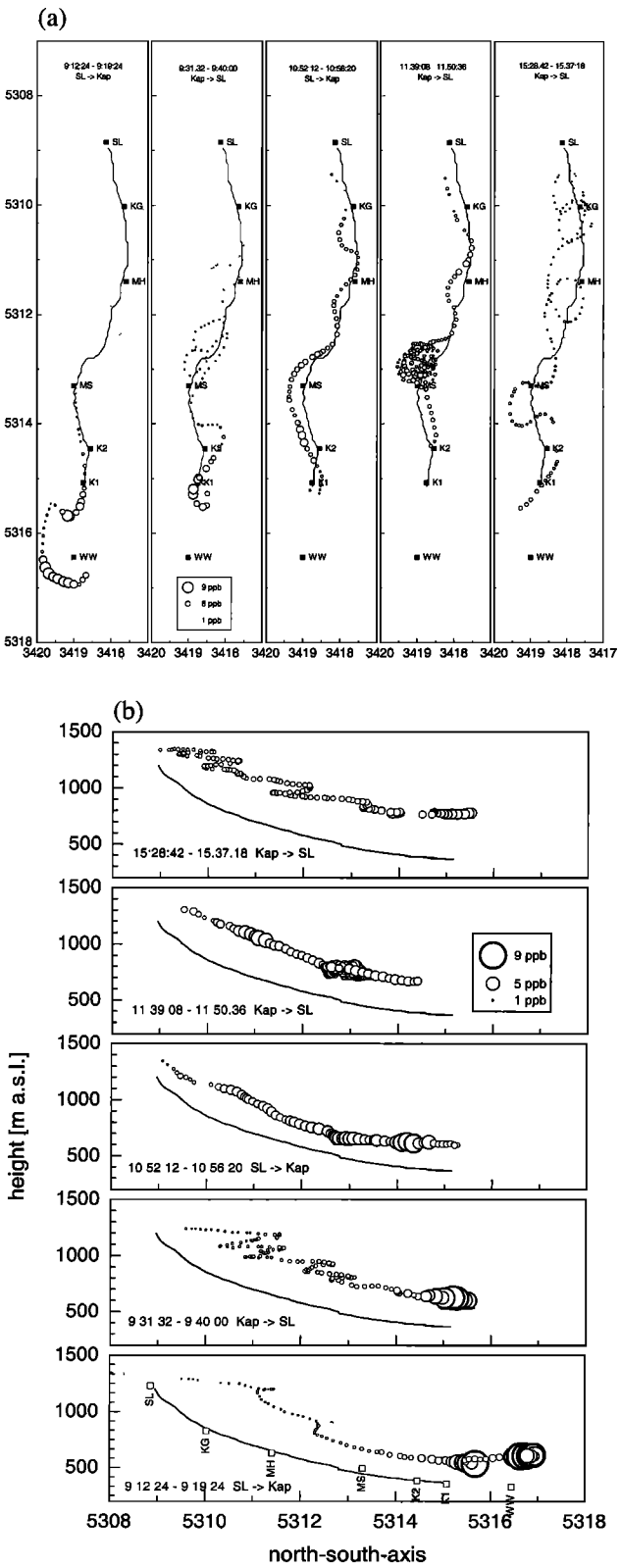

Figure 10. Concentrations of NO_2 on June 5 along the flight pattern of the motor glider: (a) displayed horizontally on a map and (b) displayed as vertical cross section along the valley axis. The diameters of the "bubbles" are proportional to the NO_2 mixing ratio. The ground-based sites are shown according to the notation in Table 1.

westerly winds result from the arrival of the slope wind system which developed at the slopes of the Rhine valley in the morning and propagated eastward [*Fiedler et al.*, this issue], supported by the heating of the elevated mountain sites of the Black Forest mountains [*Kalthoff et al.*, this issue]. After 1130 CET, the air mass seen at SL was not advected from the valley anymore but directly from the Rhine valley. Ozone at KG is rather constant throughout the mixed valley wind layer and increased gradually from profile to profile. The influence of air advected from the Rhine valley is seen in the relatively strong increase of ozone over the three profiles collected between 1231 and 1431 CET. Only a shallow layer at the surface remained at lower mixing ratios. This vertical ozone gradient increased in the evening when the surface layer became stably stratified again. At 1802 CET, ozone was approximately 80 ppb at 850 msl but only 60 ppb at the ground. At this time the southerly winds in the lowest levels indicated the onset of the nocturnal mountain winds.

3.3. Airborne Measurements

The onset and duration of the valley wind system on the June 5 is also seen in the data from the aircraft. Figure 10 presents the NO_2 mixing ratios measured between 0900 and 1540 CET and plotted along the flight tracks in the valley. Enhanced NO_2 mixing ratios (up to 10 ppb) are found in the first flight over the Zarten Basin and at the entrance to the valley. The sequence of flights along the valley clearly documents the transport and dilution of the polluted air in the morning. The meandering shape of the flight patterns within the valley was necessary for ascending the relatively steep valley and in order to allow for the sampling time of 10 min for the in situ measurements of VOCs (see B. Kolahgar et al., unpublished manuscript, 1999).

Only a relatively small fraction of the total data set obtained by the aircraft is presented here. The full flight patterns included a vertical sounding near K2, horizontal transects at altitude, and excursions to the Rhine Valley, where the airplane was stationed. The highest ozone mixing ratios (up to 110 ppb) were observed in the Rhine valley. This supports the conclusion from the vertical soundings that the enhanced ozone levels observed in the afternoon at Schauinsland were advected from the Rhine valley.

4. Discussion

Figure 5 reveals the good correlation between ozone and temperature that also has been observed at many monitoring stations. At Schauinsland the correlation is good on longer timescales, that is, periods of a week or so. A rather simple explanation is that both ozone and temperature are the result of radiation (photochemistry and heating, respectively). In addition, temperature influences precursor emissions (in particular biogenic VOCs) and rate coefficients. Weak winds and stable stratification also tend to enhance both temperature and photooxidant formation. On a diurnal scale the largest ozone increase is seen on days with both strong insolation and high precursor concentrations. This provides strong evidence for the small-scale nature of the high ozone levels observed at Schauinsland in such situations.

4.1. Partitioning of NO_y at Schauinsland

The diurnal variation of the mixing ratios of different NO_y components: NO_x, NO_y, NO_z (= NO_y − NO_x), HNO_3, and

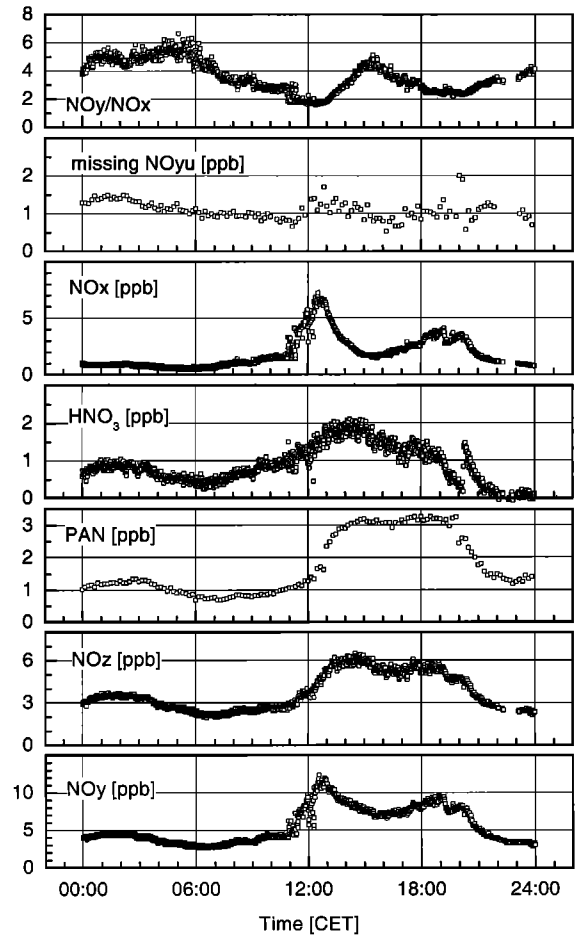

Figure 11. Mixing ratios of odd-nitrogen compounds on June 5 at SL.

PAN, as well as the concentration ratio NO_y/NO_x at Schauinsland, is shown in Figure 11. The mixing ratios of all NO_y components increase shortly before noon due to the arrival of polluted air to the site. After this time, the NO_y/NO_x ratio increases strongly due to chemical aging of the air mass: The mixing ratio of NO_x decreases rapidly, whereas the photochemical products of NO_x, that is, NO_z, HNO_3, and PAN, continue to increase. The HNO_3 concentration is derived indirectly from the difference of the NO_y measurements with and without the denuder and thus may contain small contributions from other soluble NO_y compounds, for example, hydroxy-substituted organic nitrates. Contributions from NO_3 and N_2O_5 should be insignificant during daytime. During or immediately after rainfall the two NO_y channels agree within ± 0.3 ppb lending confidence to the measurement of insoluble NO_y.

The mixing ratio of insoluble NO_y (NO_{yu}) is about 1 ppb larger than the sum of NO_x and PAN. The missing fraction of NO_{yu} (second panel in Figure 11) is likely due to organic nitrates other than PAN, which were not measured in SLOPE96. *Flocke et al.* [1998] found C_1-C_8 alkyl nitrates at mixing ratios up to 600 ppt during long-term measurements between 1990 and 1992 at Schauinsland. On average, alkyl nitrates comprised approximately 3% of NO_y with little seasonal variation. For the air mass encountered during early afternoon, alkyl nitrates would be expected to explain about 30% of the missing NO_{yu}. During the Southern Oxidant Study (SOS), mixing ratios of peroxypropionic nitric anhydride (PPN) and peroxymethacrylic nitric anhydride (MPAN) were observed to reach about 450 and 300 ppt in the presence of 3 ppb PAN [*Williams et al.*, 1997]. When assuming similar ratios for Schauinsland, the missing NO_{yu} could be entirely explained by PAN homologues and alkyl nitrates.

4.2. Estimation of [OH] From HNO_3 Formation at Schauinsland

Reaction of NO_2 with OH (R3) represents the major loss process for NO_x and the major source of HNO_3 in the sunlit atmosphere.

$$\text{(R3)} \qquad NO_2 + OH + (M) \rightarrow HNO_3 + (M)$$

Under the assumption that the rate of change of $[NO_2]$ is exclusively due to local photochemistry (i.e., homogeneous and quasi-stationary conditions), equation (5), where k_3 is the rate coefficient for reaction (R3), can be used to obtain an estimate of the OH concentration from the observed changes in HNO_3 and NO_2.

$$\frac{d[HNO_3]}{dt} = [NO_2] \times [OH] \times k_3 \qquad (5)$$

The assumption implies that the NO_y mixing ratio should remain constant. However, NO_y decreases from 9.2 to 7.8 ppb in the time interval between 0130 and 0300 CET, whereas PAN remains constant. Possible explanations are mixing of air masses with different chemical composition or NO_y losses due to dry deposition of HNO_3. The first explanation would preclude information about the "true" OH concentration in the air mass, as the measured decrease in NO_2 and the simultaneous increase in HNO_3 could be the result of admixture of photochemically aged air with a larger HNO_3 to NO_2 ratio, for example, from aloft. The estimate would then simply give an upper limit for [OH].

The potential influence of HNO_3 deposition is examined with a simple model solving the balance equations for all measured NO_y species (equation (6)). A first-order loss term (k_D) is included to account for the deposition of HNO_3. The model is constrained by observed values for PAN and the NO/NO_2 ratio (smoothed by fitting second-order polynomials). A constant mixing ratio of 1 ppb (about 10% of NO_y) is included to account for the missing NO_{yu} compounds as described above. The OH concentration and the deposition coefficient in the model are then varied in order to find the best description of the measured time dependence of the NO_2 and HNO_3 mixing ratio.

$$\frac{d[HNO_3]}{dt} = [NO_2] \times [OH] \times k_3 - [HNO_3] \times k_D$$

$$\frac{d[NO_2]}{dt} = -[NO_2] \times [OH] \times k_3 - \frac{d[PAN]}{dt}$$

$$\frac{d[PAN]}{dt} \qquad \text{(from fit to measurements)} \qquad (6)$$

$$\frac{d[NO]}{dt} = \frac{d[NO_2]}{dt} \times \frac{[NO]}{[NO_2]}$$

$$\cdot \text{ (with } NO/NO_2 \text{ ratio from measurements)}$$

$$\frac{d[NO_y]}{dt} = \frac{d[HNO_3]}{dt} + \frac{d[NO_2]}{dt} + \frac{d[NO]}{dt} + \frac{d[PAN]}{dt}$$

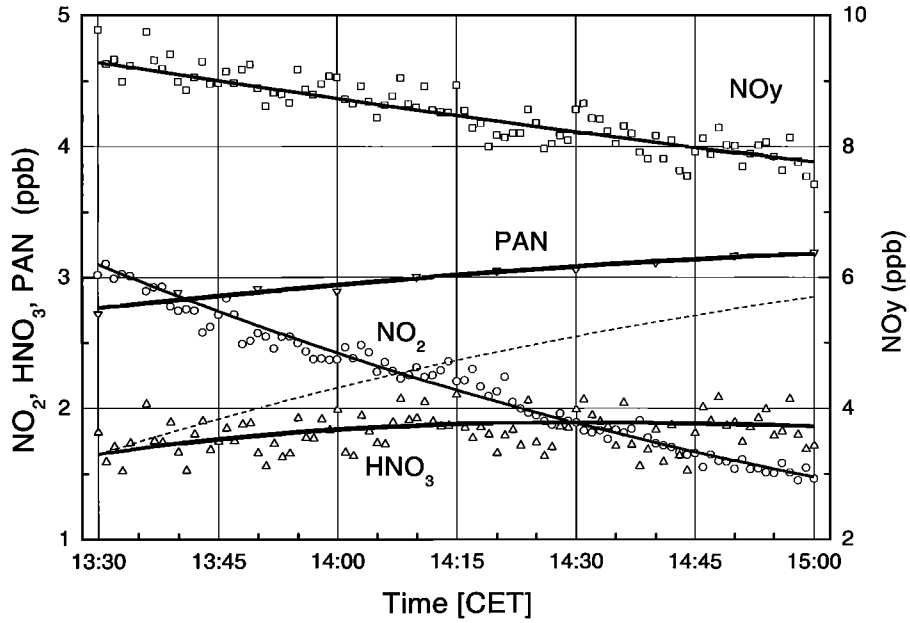

Figure 12. Comparison of model results (solid lines) with the data for NO_2 (open circles), HNO_3 (open triangles), and NO_y (open squares) from June 5 at Schauinsland. Model parameters: k_3: 9×10^{-12} cm^3 s^{-1}, $k_D(HNO_3) = 9 \times 10^{-5}$ s^{-1}, [OH] = 1.1×10^7 cm^{-3}. [PAN] (downward pointing triangles) is not calculated in the model but fitted to the measurement.

The model results are displayed in Figure 12 together with the measurements. With the recently revised value for k_3 (9×10^{-12} cm^3 s^{-1} at 1 bar [*Donahue et al.*, 1997]), an OH concentration of 1.1×10^7 cm^{-3} is required to describe the temporal change of NO_2. Without deposition (dashed line), HNO_3 increases too rapidly in the model. The measured change of both HNO_3 and NO_y is best described with a first-order deposition coefficient for HNO_3 of $k_D = 9 \times 10^{-5}$ s^{-1}. With a scale height of about 350 m as estimated from the vertical soundings at KG, this corresponds to a deposition velocity for HNO_3 of approximately 3 cm s^{-1}, which is within the range of measured values [*Huebert*, 1980; *Munger et al.*, 1996]. The OH concentration is somewhat smaller than what would be obtained by simply solving equation (5) because some of the NO_2 losses go into the formation of PAN. When including dry deposition of NO_2 with a relatively high deposition velocity of 0.5 cm s^{-1} [cf. *Munger et al.*, 1996, Figure 10], the resulting OH concentration decreases to slightly less than 10^7 cm^{-3}. Adopting the same deposition velocity for PAN, [OH] is further reduced to 8×10^6 cm^{-3}, and the deposition velocity required to match the observed HNO_3 concentrations decreases to about 2.5 cm s^{-1}.

Although we should like to reemphasize the indirect nature of our estimate, the analysis reveals a consistent picture of the NO_y partitioning. The OH concentration is similar to that derived from the degradation of VOCs and NO_x during transport between Kappel and Schauinsland [*Volz-Thomas and Kolahgar*, this issue]. These authors obtain [OH] = 7×10^6 cm^{-3} for the time interval 0930–1130 CET in the presence of similar values for J_{O1D} (see Figure 7) and in the presence of NO_2 mixing ratios between 3 and 15 ppb. They also compare their results with other measurements and discuss the radical budget.

4.3. Photostationary State (PSS) of NO_x at Schauinsland

In several studies the local ozone formation rate was estimated from the photostationary state of NO_x, that is, from the reaction cycle below under the assumption that quasi steady state is established and that (R4) and (R5) are the rate-limiting steps in the formation of ozone [cf. *Cantrell et al.*, 1993; *Kelly et al.*, 1980; *Kleinman et al.*, 1995; *Parrish et al.*, 1986; *Ridley et al.*, 1992; *Volz et al.*, 1988; *Volz-Thomas et al.*, 1997].

(R1) $NO_2 + h\nu + O_2 \rightarrow NO + O_3$

(R2) $NO + O_3 \rightarrow NO_2 + O_2$

(R4) $NO + RO_2 \rightarrow NO_2 + RO$

(R5) $NO + HO_2 \rightarrow NO_2 + OH$

The approach neglects the formation of alkyl nitrates (usually a small term) and assumes that all of the NO oxidation that does not occur via reaction with O_3 gives rise to ozone formation. In this sense, $P(O_3)$ as calculated from (7) is an upper limit of the photochemical ozone formation rate.

$$P(O_3) = J_{NO_2} \times [NO_2] - [NO] \times [O_3] \times k_2 \qquad (7)$$

As is seen from Figure 5, $P(O_3)$ as calculated from (7) exhibits a pronounced diurnal cycle with maximum values around noontime. The highest production rates of about 60 ppb/h occur at times when high precursor concentrations coincide with large values of the actinic flux (i.e., J_{NO_2}). This behavior is highlighted in Figure 13, where the NO_x mixing ratio and J_{NO_2}, which are both available at high time resolution, are used as proxy for these quantities. $P(O_3)$ increases linearly with $J_{NO_2} \times [NO_x]$, with a slope of approximately 0.25 (ppb h^{-1} per ppb h^{-1}). This value is consistent with earlier observations at Schauinsland and at the TOR stations Rørvik and Izaña [*Volz-Thomas et al.*, 1997]. For the highest NO_x mixing ratios, $P(O_3)$ tends to level off due to the transition from NO_x-limited to NO_x-saturated conditions.

In earlier studies [*Volz-Thomas et al.*, 1997] the ozone formation rate obtained from (7) at SL was found to be about a

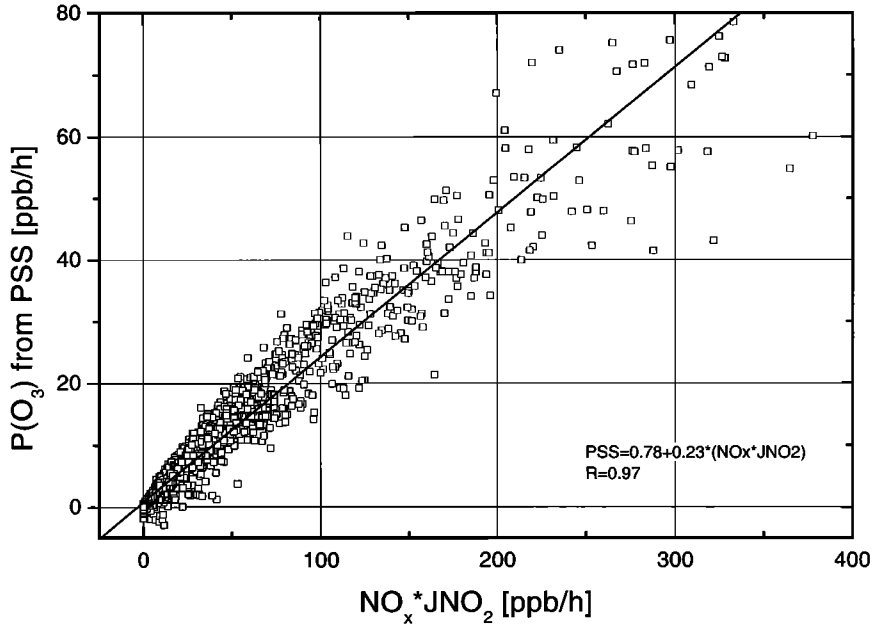

Figure 13. Ozone formation rate as estimated from PSS (equation (7)) as a function of the product of J_{NO_2} and NO_x mixing ratio. The slope of 850 ppb h^{-1} per ppb s^{-1} is similar to that reported earlier for Schauinsland and for other TOR sites [*Volz-Thomas et al.*, 1997].

factor of 3 higher than that calculated from the concentrations of NO and of peroxy radicals measured by Matrix Isolation and Electron Spin Resonance (MIESR) [*Mihelcic et al.*, 1990]. On the other hand, relatively good agreement between the two methods was observed in relatively clean air at Izaña, that is, at NO_x concentrations below 2 ppb [*Volz-Thomas et al.*, 1997]. A comparison of PSS-derived peroxy radical concentrations with measurements made by chemical amplification during the ROSE study [*Cantrell et al.*, 1993] revealed relatively good agreement on 1 day, whereas a similar difference as at Schauinsland was observed on another day. $P(O_3)$ from PSS reached noontime values of about 10 ppb/h in the presence of 1 ppb of NO_x, giving a similar ratio of about 0.25–0.3 (ppb h^{-1} per ppb h^{-1}) as found at Izaña and SL. The reason for the large discrepancy between PSS-derived peroxy radicals and direct measurements at Schauinsland, which seems to increase with increasing NO_x mixing ratio, is at present unclear and will be subject to further investigations.

5. Conclusions

During SLOPE96, measurements of chemical trace constituents were made at ground-based sites, on tethered balloons, and aboard a small aircraft. Intercomparison experiments helped to remedy a few calibration problems and ensured the consistency of the data set.

A valley wind system that was sufficient to transport pollutants from Freiburg and the Rhine valley to the Schauinsland was in effect only on 1 day, June 5. The polluted air mass was clearly identified by all measurement platforms. The large number of measurements provided a clear picture of the situation.

An OH concentration of 8×10^6 cm^{-3} is estimated from the local NO_2 decay and HNO_3 formation at Schauinsland under the assumption of stationary conditions, similar to that derived from the degradation of hydrocarbons during transport from Kappel to Schauinsland in the morning of the same day. The local ozone production rate as derived from PSS reached maximum values of 60 ppb/h and showed a good correlation with the product of J_{NO_2} and NO_x, similar to earlier observations at Schauinsland and at other sites.

Acknowledgments. The campaign was partially funded by BMBF as part of the EUROTRAC subproject TOR (grant 07 EU 723 A/5). Thanks are due to all SLOPE96 enthusiasts who successfully supported the campaign with various measurements. We are grateful to the staff of the Umweltbundesamt, Meßstelle Schauinsland, for their cooperation and hospitality during the campaign. We also thank Sabine Jansen for her assistance in data handling and preparation of Figure 1 and the Central Chemistry Lab (ZCH) of FZJ for the nitrate analyses. The instruments for NO_2 and O_3 aboard the MetAir aircraft were supplied and calibrated by the Paul Scherrer Institute (PSI, Villigen, Switzerland). The authors would like to thank the reviewers of the manuscript for their helpful and constructive comments.

References

Baumbach, G., K. Baumann, A. Grauer, R. Semmler, and B. Steisslinger, A tethersonde measuring system for detection of O_3, NO_2, hydrocarbon concentrations, and meteorological parameters in the lower planetary boundary layer, *Meteorol. Z.*, *2*, 178–188, 1993.

Burrows, J. P., et al., The Global Ozone Monitoring Experiment (GOME): Mission concept and first scientific results, *J. Atmos. Sci.*, *56*, 151–175, 1999.

Cantrell, C. A., et al., Peroxy radicals as measured in ROSE and estimated from photostationary state deviations, *J. Geophys. Res.*, *98*, 18,355–18,367, 1993.

Dasgupta, P. K., S. Dong, H. Hwang, H. C. Yang, and Z. Genfa, Continuous liquid-phase flourometric coupled to a diffusion scrubber for the real-time determination of atmospheric formaldehyde, hydrogen peroxide and sulfur dioxide, *Atmos. Environ.*, *22*, 949–963, 1988.

Davidson, J. A., C. A. Cantrell, A. H. McDaniel, R. E. Shetter, S. Madronich, and J. G. Calvert, Visible-ultraviolet absorption cross sections for NO_2 as a function of temperature, *J. Geophys. Res.*, *93*, 7105–7112, 1988.

DeMore, W. B., S. P. Sander, D. M. Golden, R. F. Hampson, M. J. Kurylo, C. J. Howard, A. R. Ravishankara, C. E. Kolb, and M. J.

Molina, Chemical kinetics and photochemical data for use in stratospheric modeling, Jet Propul. Lab., Pasadena, Calif., 1994.

DeMore, W. B., S. P. Sander, D. M. Golden, R. F. Hampson, M. J. Kurylo, C. J. Howard, A. R. Ravishankara, C. E. Kolb, and M. J. Molina, Chemical kinetics and photochemical data for use in stratospheric modeling, 266 pp., Jet Propul. Lab., Pasadena, Calif., 1997.

Donahue, N. M., M. K. Dubey, R. Mohrschladt, L. D. Kenneth, and J. G. Anderson, High-pressure flow study of the reactions OH + $NO_x \rightarrow HONO_x$, *J. Geophys. Res.*, *102*, 6159–6168, 1997.

Fahey, D. W., C. S. Eubank, G. Hübler, and F. C. Fehsenfeld, Evaluation of a catalytic reduction technique for the measurement of total reactive odd-nitrogen NO_y in the atmosphere, *J. Atmos. Chem.*, *3*, 435–468, 1985.

Fehsenfeld, F. C., et al., A ground-based intercomparison of NO, NO_x, NO_y measurement technique, *J. Geophys. Res.*, *92*, 14,710–14,722, 1987.

Fiedler, F., I. Bischoff-Gauß, N. Kalthoff, and G. Adrian, Modeling of the transport and diffusion of a tracer in the Freiburg-Schauinsland area, *J. Geophys. Res.*, this issue.

Flocke, F., A. Volz-Thomas, H.-J. Buers, H. W. Pätz, H.-J. Garthe, and D. Kley, Long-term measurements of alkyl nitrates in southern Germany, 1, General behavior, seasonal and diurnal variation, *J. Geophys. Res.*, *103*, 5729–5746, 1998.

Gardner, E. P., P. D. Sperry, and J. G. Calvert, Primary quantum yields of NO_2 photodissociation, *J. Geophys. Res.*, *92*, 6642–6652, 1987.

Gerbig, C., D. Kley, A. Volz-Thomas, J. Kent, K. Dewey, and D. S. McKenna, Fast-response resonance fluorescence CO measurements aboard the C-130: Instrument characterization and measurements made during NARE '93, *J. Geophys. Res.*, *101*, 29,229–29,238, 1996.

Güsten, H., G. Heinrich, R. W. H. Schmidt, and U. Schurath, A novel ozone sensor for direct eddy flux measurements, *J. Atmos. Chem.*, *14*, 73–84, 1992.

Harris, G. W., I. G. Mackay, T. Iguchi, L. K. Mayne, and H. I. Schiff, Measurements of formaldeyde in the troposphere by tunable diode laser absorption spectroscopy, *J. Atmos. Chem.*, *8*, 119–137, 1989.

Hofzumahaus, A., A. Kraus, and M. Müller, Solar actinic flux spectroradiometry: A technique for measuring photolysis frequencies in the atmosphere, *Appl. Opt.*, *38*, 4443–4460, 1999.

Huebert, B. J., Nitric acid and aerosol nitrate measurements in the equatorial Pacific region, *Geophys. Res. Lett.*, *7*, 325–328, 1980.

Kalthoff, N., V. Horlacher, U. Corsmeier, A. Volz-Thomas, B. Kolahgar, M. Möllmann-Coers, and A. Knaps, Influence of valley winds on transport and dispersion of airborne pollutants in the Freiburg-Schauinsland area, *J. Geophys. Res.*, this issue.

Kelly, T. J., D. H. Stedman, J. A. Ritter, and R. B. Harvey, Measurements of oxides of nitrogen and nitric acid in clean air, *J. Geophys. Res.*, *85*, 7417–7425, 1980.

Kern, T., D. Kley, and D. Klemp, Messungen der Mischungsverhältnisse des Formaldehyds in belasteter Troposphäre mittels Spektroskopie mit abstimmbaren Diodenlasern—Untersuchungen zur Bedeutung des Formaldehyds für die Ozonproduktion aus Kfz-Abgasen, *Rep. Jül-3143*, Forsch. Jülich, Jülich, Germany, 1995.

Kern, T., D. Klemp, D. Kley, and T. Schmitz, Measurements of atmospheric formaldehyde concentrations under conditions of the Polluted Troposphere by Tunable Diode Laser Absorption Spectroscopy (TDLAS)—A contribution to EUROTRAC-subproject TOR, in *EUROTRAC Symposium*, edited by P. M. Borrell et al., pp. 1013–1018, Comput. Mech., Billerica, Mass., 1996.

Kleinman, L., Y. N. Lee, S. R. Springston, J. H. Lee, L. Nunnermacker, J. Weinstein-Lloyd, X. L. Zhou, and L. Newman, Peroxy radical concentration and ozone formation rate at a rural site in the southeastern United States, *J. Geophys. Res.*, *100*, 7263–7273, 1995.

Klemp, D., T. Kern, H. Beck, and D. Mihelcic, Design and development of a one-channel tunable diode laser spectrometer for the measurement of atmospheric formaldehyde mixing ratios—A contribution to EUROTRAC-subproject JETDLAG, in *EUROTRAC Annual Report 1993*, pp. 17–25, Int. Sci. Secr. Fraunhofer Inst. (IFU), Garmisch-Partenkirchen, Germany, 1994.

Kley, D., J. Beck, P. I. Grennfelt, Ø. Hov, and A. S. Penkett, Tropospheric Ozone Research (TOR)—A sub-project of EUROTRAC, *J. Atmos. Chem.*, *28*, 1–9, 1997.

Kramp, F., and A. Volz-Thomas, On the budget of OH radicals and ozone in an urban plume from the decay of C5-C8 hydrocarbons and NO_x, *J. Atmos. Chem.*, *28*, 263–282, 1997.

Lazrus, A. L., G. L. Kok, J. A. Lind, S. N. Gitlin, B. G. Heikes, and R. E. Shetter, Automated fluormetric method for hydrogen peroxide in air, *Anal. Chem.*, *58*, 594–597, 1986.

Lazrus, A. L., K. L. Fong, and J. A. Lind, Automated fluorometric determination of formaldehyde in air, *Fresenius J. Anal. Chem.*, *60*, 1074–1078, 1988.

Leighton, P. A., *Photochemistry of Air Pollution*, Academic, San Diego, Calif., 1961.

Madronich, S., Photodissociation in the atmosphere: Actinic flux and the effects of ground reflections and clouds, *J. Geophys. Res.*, *92*, 9740–9752, 1987.

Michelsen, H. A., R. J. Salawitch, P. O. Wennberg, and J. G. Anderson, Production of $O(^1D)$ from photolysis of O_3, *Geophys. Res. Lett.*, *21*, 2227–2230, 1994.

Mihelcic, D., A. Volz-Thomas, H. W. Pätz, D. Kley, and M. Mihelcic, Numerical analysis of ESR spectra from atmospheric samples, *J. Atmos. Chem.*, *11*, 271–297, 1990.

Molina, L. T., and M. J. Molina, Absolute absorption cross section of ozone in the 185- to 350-nm wavelength range, *J. Geophys. Res.*, *91*, 14,501–14,508, 1986.

Moortgart, G. K., W. Seiler, and P. Warneck, Photodissociation of HCHO in air: CO and H2 quantum yields at 220 and 300 K, *J. Chem. Phys.*, *78*, 1185–1190, 1983.

Munger, J. W., S. C. Wofsy, P. S. Bakwin, S.-M. Fan, M. L. Goulden, B. C. Daube, A. H. Goldstein, K. E. Moore, and D. R. Fitzjarrald, Atmospheric deposition of reactive nitrogen oxides and ozone in a temperate deciduous forest and subarctic woodland, 1, Measurements and mechanisms, *J. Geophys. Res.*, *101*, 12,639–12,657, 1996.

Neininger, B., M. Bäumle, O. Liechti, and M. Lehning (Eds.), Airborne measurements of air pollution in the regions of Geneva, and Berne, 1996–1997, Swiss Agency for the Environ., For. and Landscape (SAEFL), Berne, 1999.

Parrish, D. D., M. Trainer, E. J. Williams, D. W. Fahey, G. Hübler, C. S. Eubank, S. C. Liu, P. C. Murphy, D. L. Albritton, and F. C. Fehsenfeld, Measurements of the NO_x-O_3 photostationary state at Niwot Ridge, Colorado, *J. Geophys. Res.*, *91*, 5361–5370, 1986.

Ridley, B. A., S. Madronich, R. B. Chatfield, J. G. Walega, R. E. Shetter, M. A. Carroll, and D. D. Montzka, Measurements and model simulations of the photostationary state during the Mauna Loa Photochemistry Experiment: Implications for radical concentrations and ozone production and loss rates, *J. Geophys. Res.*, *97*, 10,361–10,374, 1992.

Slemr, J., Determination of volatile carbonyl compounds in clean air, *Fresenius J. Anal. Chem.*, *340*, 672–677, 1991.

Slemr, J., W. Junkermann, and A. Volz-Thomas, Temporal variations and budget of formaldehyde at a rural site in southern Germany, *Atmos. Environ.*, *3*, 3667–3676, 1996.

Stamnes, K. S., S.-C. Tsay, W. Wiscombe, and K. Jayaweera, Numerically stable algorithm for discrete-ordinate-method radiative transfer in multiple scattering and emitting layered media, *Appl. Opt.*, *27*, 2501–2509, 1988.

Verein Deutscher Ingenieure (VDI), Gaseous air pollution measurement-determination of nitrogen dioxide concentration—Photometric manual standard method (Saltzman), Beuth Verlag GmbH, Berlin, 1990.

Volz, A., D. Mihelcic, P. Müsgen, H. W. Pätz, G. Pilwat, H. Geiss, and D. Kley, Ozone production in the Black Forest: Direct measurements of RO_2, NO_x and other relevant parameters, in *Tropospheric Ozone—Regional and Global Scale Interactions*, edited by I. S. A. Isaksen, pp. 293–302, D. Reidel, Norwell, Mass., 1988.

Volz-Thomas, A., A. Lerner, H. W. Pätz, M. Schultz, D. S. McKenna, R. Schmitt, S. Madronich, and E. P. Röth, Airborne measurements of the photolysis frequency of NO_2, *J. Geophys. Res.*, *101*, 18,613–18,627, 1996.

Volz-Thomas, A., et al., Photochemical ozone production rates at different TOR sites, in *Tropospheric Ozone Research*, edited by Ø. Hov, pp. 95–110, Springer-Verlag, New York, 1997.

Volz-Thomas, A., N. Houben, A. Lerner, and H.-W. Pätz, Charakterisierung der dynamischen PAN-Kalibriereinheit der MeteorologieConsult GmbH, 8 pp., Forsch. Jülich, Jülich, Germany, 1998.

Volz-Thomas, A., and B. Kolahgar, On the budget of hydroxyl radicals at Schauinsland during SLOPE96, *J. Geophys. Res.*, this issue.

Volz-Thomas, A., H. Geiß, and N. Kalthoff, The Schauinsland Ozone Precursor Experiment (SLOPE96): Scientific background and main results, *J. Geophys. Res.*, this issue.

Williams, J., et al., Regional ozone from biogenic hydrocarbons deduced from airborne measurements of PAN, PPN, and MPAN, *J. Geophys. Res.*, *102*, 1099–1102, 1997.

U. Corsmeier and N. Kalthoff, Institut für Meteorologie und Klimaforschung, Forschungszentrum Karlsruhe, D-76131 Karlsruhe, Germany.

K. Glaser and U. Vogt, Institut für Verfahrenstechnik und Dampfkesselwesen, Universität Stuttgart, Pfaffenwaldring 23, D-70569, Stuttgart, Germany.

D. Klemp, B. Kolahgar, A. Lerner, H.-W. Pätz, T. Schmitz, and A. Volz-Thomas, Institut für Chemie und Dynamik der Geosphäre II, Forschungszentrum Jülich, Leo Brandt Straße, D-52425 Julich, Germany. (a.volz-thomas@kfa-juelich.de)

B. Neininger, MetAir AG, Länggstrasse 19, CH-8308 Illnau, Switzerland.

M. G. Schultz, Max-Planck-Institut für Meteorologie, Bundesstr. 55, 20146 Hamburg, Germany.

J. Slemr, Fraunhofer Institut für Atmosphärische Umweltforschung, Kreuzeckbahnstr. 19, D-82467 Garmisch-Partenkirchen, Germany.

(Received May 21, 1999; revised August 25, 1999;
accepted August 30, 1999.)